Tellus
SERIES B
CHEMICAL
AND PHYSICAL
METEOROLOGY
PUBLISHED BY THE INTERNATIONAL METEOROLOGICAL INSTITUTE IN STOCKHOLM

Tellus (2011), 63B, 1–22

TELLUS

Evolution of natural and anthropogenic fluxes of atmospheric CO_2 from 1957 to 2003

By CHARLES D. KEELING, STEPHEN C. PIPER*, TIMOTHY P. WHORF and RALPH F. KEELING, *Scripps Institution of Oceanography, La Jolla, CA 92093-0244, USA*

(Manuscript received 2 December 2009; in final form 26 August 2010)

ABSTRACT

An analysis is carried out of the longest available records of atmospheric CO_2 and its $^{13}C/^{12}C$ ratio from the Scripps Institution of Oceanography network of fixed stations, augmented by data in the 1950s and 1960s from ships and ice floes. Using regression analysis, we separate the interhemispheric gradients of CO_2 and $^{13}C/^{12}C$ into: (1) a stationary (possibly natural) component that is constant with time, and (2) a time-evolving component that increases in proportion to fossil fuel emissions. Inverse calculations using an atmospheric transport model are used to interpret the components of the gradients in terms of land and ocean sinks. The stationary gradients in CO_2 and $^{13}C/^{12}C$ are both satisfactorily explained by ocean processes, including an ocean carbon loop that transports 0.5 PgC yr^{-1} southwards in the ocean balanced by an atmospheric return flow. A stationary northern land sink appears to be ruled out unless its effect on the gradient has been offset by a strong rectifier effect, which seems doubtful. A growing northern land sink is not ruled out, but has an uncertain magnitude (0.3–1.7 PgC yr^{-1} centred on year 2003) dependent on the rate at which CO_2 from fossil fuel burning is dispersed vertically and between hemispheres.

1. Introduction

In the early 1950s, an international group of scientists proposed a scheme to gather data in the geophysical disciplines on a comprehensive scale never before attempted. The International Geophysical Year (IGY) of 1957–1958 was the outcome. Although focused on the physical properties of the Earth, the IGY took on the then even low-ranking issue of climate change, and as a minor example, the study of atmospheric CO_2 (Weart, 2003). Atmospheric CO_2 was suspected to be increasing in concentration globally but proof was lacking owing to large scatter in the existing data. New technologies, however, were adding incentives to resolve such uncertainties, including gas analysers that could automatically register changes in CO_2 concentration when calibrated with gas mixtures of known concentration. With logistical and financial support provided by the IGY, CO_2 data gathering began at fixed stations, on ice floes, on oceanic expeditions and on aircraft flights. By the close of the IGY, seasonal and latitudinal variability in atmospheric CO_2 were broadly documented to a precision close to that attainable today.

After the IGY, it seemed clearly desirable to continue these measurements, and although the effort was reduced in scope, by 1960, data showed that atmospheric CO_2 concentrations each year were higher than the year before. The natural carbon cycle was being altered globally by human activity. The study continued, and by 1970 showed worldwide increases in concentration, almost undeniably related to fossil fuel combustion. An international program was then established by the World Meteorological Organization to support long-term measurements of atmospheric CO_2 worldwide especially at fixed stations. Today more than 100 of these are operating, 10 of which, with antecedents to the original IGY program, provide the data central to this paper.

Records at four of these stations, three in the Northern Hemisphere (Barrow, La Jolla and Mauna Loa) and one at the South Pole, constitute, with additional IGY data, a history of CO_2 variations from the Arctic to the Antarctic over a span of 50 yr. During this time interval, emissions of CO_2 from fuel combustion increased from 2.3 thousand million metric tons per year (PgC yr^{-1}) to 7.3 PgC yr^{-1} in 2003 (Marland et al., 2005). Of the CO_2 released, 90% was injected into the Northern Hemisphere where it lingered before mixing fully worldwide. The CO_2 concentration, in response, rose faster in the Northern Hemisphere than in the southern, the interhemispheric difference increasing from near zero during the IGY to about three parts per million by volume (ppm) in 2003 (Keeling et al., 2005).

Here we use this fact to diagnose how the carbon cycle has evolved over the past half century. As noted in earlier studies,

*Corresponding author.
e-mail: scpiper@ucsd.edu
DOI: 10.1111/j.1600-0889.2010.00507.x

the CO_2 concentration measured at fixed stations, except for short-term variability, has risen approximately in proportion to the rate of fossil fuel CO_2 emissions (Keeling et al., 1989a). The overall CO_2 rise since 1958 is well explained assuming 56% of the fossil fuel emissions remain airborne. To maintain this proportionality requires that the exchange of CO_2 between the atmosphere and the land and oceans, which must account for the remainder, has varied in close relation to fossil fuel CO_2 emissions. This is possible because any direct response of the oceans and land plants to rising CO_2 can be expected to scale roughly with rate of rise of CO_2 and because human population growth, economic activity, agriculture and forest practices have all increased steadily over the past half century, as have fossil fuel emissions. The CO_2 data suggest that human activities have directly or indirectly caused most of the long-term changes in CO_2 fluxes between the atmosphere and the terrestrial biosphere and the oceans.

These recent human-induced carbon fluxes are superimposed on fluxes that have remained largely unchanged over the past half century. As noted in prior work, the apparent time-varying latitudinal gradient in CO_2 between stations does not vanish when the data are extrapolated to zero fossil fuel emissions (Keeling et al., 1989a), indicating the presence of a gradient of presumably natural origin over the record period. Aided by CO_2 records that extend back to when fossil fuel emissions were relatively small, we seek to identify the fluxes causing this stationary gradient, or at least their relative terrestrial and oceanic fractions.

Although our approach emphasizes the dominant contributors to the interhemispheric gradient in atmospheric CO_2 arising from a combination of fluxes that are nearly stationary and fluxes that have varied approximately in proportion to variations in fossil fuel CO_2 emissions, we recognize that additional variability is also discernable in the CO_2 data. Short-term natural variability related to El Niño events is unmistakable. On longer time-scales, also expected is natural variability and possibly even variability related to human impacts, which have not changed in proportion to fuel emission increases. These contributions to variability, which may also be of interest, are neglected in this analysis.

2. Description of data

Atmospheric CO_2 concentration data used here, as summarized in Table 1, are as reported by Keeling et al. (1989a,b, 2005). All data are reported on the Scripps X03 calibration scale (Bacastow et al., 1985). Beginning in 1978, the isotopic ratio, $^{13}C/^{12}C$, of CO_2 was also measured on flask samples, at first for only a few stations of our array, but by 1986 at all stations (Keeling et al., 1989a; Keeling et al., 2005). These data are expressed as the reduced ratio, $\delta^{13}C = R_i/R_o - 1$, where R_i and R_o denote, respectively, the $^{13}C/^{12}C$ of the sampled air and of the international standard, Pee Dee Belemnite (PDB).

Each concentration and isotopic data set has been seasonally adjusted, and smoothed by a spline fit with a controlled average of its second derivative (Bacastow et al., 1985) to provide interannually varying time series consistent in smoothness from station to station. To produce estimates of latitudinal gradients, we subtract spline fits for each station from spline fits for the South Pole. To allow calculations at the monthly resolution, annual global fossil fuel emissions of CO_2, mainly from fossil fuel but including CO_2 emissions from cement production (Marland et al., 2005) (we will use 'fossil fuel (ff)' to refer to fossil fuel plus cement production hereinafter), were fit to a spline and adjusted so that calendar year averages match the reported averages.

3. Regression analysis

3.1. Methods

Following earlier studies (Keeling et al., 1989a; Conway and Tans, 1999; Fan et al., 1999; Taylor and Orr, 2000), we determine a relation between the atmospheric CO_2 gradient and fossil fuel CO_2 emissions, by performing a linear regression between the observed concentration difference, in ppm, between the South Pole and any other station, i, onto fossil fuel emissions, ff, in PgC yr^{-1}. The observed concentration difference, ΔC_i(obs), is computed as the difference of C_i, the concentration at station i determined from a spline fit of the original observations, from C_o, the equivalent concentration from the South Pole. Over the time interval of measurements for station i, we obtain by a least squares procedure (Bevington, 1969) the linear relation

$$\Delta C_i(\text{fit}) = S_i \times \text{ff} + \Delta C_i(\text{res}), \tag{1}$$

where ΔC_i(fit) is the predicted CO_2 concentration difference, ff denotes fossil fuel emissions in PgC yr^{-1}; S_i a slope function in ppm/(PgC yr^{-1}) and ΔC_i(res), a time-invariant global constant that reflects a component of the gradient that has remained stationary over the observation period. The product, $S_i \times$ ff, will also be designated by the symbol ΔC_i(ff). A glossary of terms and descriptors used in this paper is presented in Table 2. We similarly fit the differences in the isotopic ratio, $\Delta\delta_i$, to the functional form

$$\Delta\delta_i(fit) = (S_i \times \text{ff}) \times (\varepsilon_{\text{ff}} - \delta_o)/(C_o + (S_i \times \text{ff})) + \Delta\delta_i(\text{res}), \tag{2}$$

where $\Delta\delta_i$(fit) is the predicted isotopic ratio difference, δ_o and C_o are the time-varying reduced isotopic ratio and CO_2 concentration, respectively, at the South Pole, ε_{ff} is the time-varying reduced isotopic ratio of fossil fuel from Andres et al. (1996a), $\Delta\delta_i$(res) is a time-invariant constant that reflects the stationary component of the $\delta^{13}C$ gradient. Equation 2 accounts for the 'dilution' of $\delta^{13}C$ by the addition of industrial CO_2 to the atmosphere, using the additivity rule for combining abundances of

Table 1. Atmospheric CO_2 concentration observations from fixed stations, ships and ice floes

Station name	Location	Time period for CO_2 observations	Time period for $\delta^{13}C$ observations
Alert, Northwest Territories, Canada (ALT)	82.3°N, 62.3°W, 210 m	May 1985–2003	May 1985–2003
Point Barrow, Alaska and vicinity (PTB)			
Ice floes A and B	A: 83.7–85.4°N, 153.5–169.6°W; B: 80.3–81.0°N, 109.1–114.8°W	1957–1958	–
Site 1–Ocean beach[a]		July 1961–Oct 1963	–
Site 2–North Meadow Lake field station[a]		Jan 1965–Sept 1967	–
Site 3–Current location	71.3°N, 156.6°W, 11 m	Jan 1974–2003	April 1982–2003
La Jolla pier, California (LJO)	32.9°N, 117.3°W, 10 m	1958–1962, Feb 1969–2003	April 1978–2003
Mauna Loa Observatory, Hawaii (MLO)	19.5°N, 155.6°W, 3397 m	March 1958–2003	Feb 1980–2003
Cape Kumukahi, Hawaii (KUM)	19.5°N, 154.8°W, 3 m 15–21.5°N(1962), 15.9–24.5°N(1968)	1962[b], 1968, March 1979–2003	Feb 1980–2003
Christmas Island, Kiribati (CHR)	2.0°N, 157.3°W, 2 m 0–7.5°N(1962), 0–4.0°N(1968)	1962[b], 1968, Dec 1974–2003	Aug 1977–2003
American Samoa (SAM)	14.2°S, 170.6°W, 30 m 12.5–17°S (1962), 11.4–18°S (1968)	1962[b],1968,Sept 1981–2003	Feb 1984–2003
Kermadec Island (KER)	29.2°S, 177.9°W, 2 m 24–34.2°S (1967–8)	1967–1968[c], Dec 1982–2003	March 1984–2003
Baring Head, New Zealand (NZD)	41.4°S, 174.9°E, 85 m 43.5–63°S (1962), 28.4–53°S (1968)	1962[d], 1968, July 1977–2003	May 1985–2003
South Pole (SPO)	90.0°S, 2810 m	July 1957–2003	March 1977–2003

[a]In situ data reported by Kelley (1969), with corrections including for carrier gas effect.
[b]Forced to fit average of 1962 and 1968 points in 1965.
[c]Observations from the NOVA ship expedition, 24°S–34.2°S.
[d]1962, 1968 observations made on the Eltanin ship expedition.

CO_2 having different isotopic ratios (Mook et al., 1983). In principle, eq. (2) could be fit for two parameters, S_i and $\Delta\delta_i$(res), but because the $\delta_{13}C$ records are too short, we instead fit only one parameter, $\Delta\delta_i$(res), and adopt the value for S_i obtained from the fit for CO_2 concentration eq. (1). The use of eq. (2) to derive the stationary component of the $\delta^{13}C$ gradient [$\Delta\delta_i$(res)] is further validated in Appendix A.

3.2. Results

Our most robust record of the latitudinal gradient in atmospheric CO_2 is for the station pair, Mauna Loa Observatory Hawaii (MLO) and the South Pole (SPO), graphed versus time in Fig. 1a. The stationary concentration difference, for MLO minus SPO, found by regression for data up to 1989, was −0.82 ppm (Keeling et al., 1989a), in close agreement with −0.87 ppm for data extended to 2003. The close agreement demonstrates that the Mauna Loa–South Pole difference has remained closely proportional to fossil fuel emissions, and thus is well approximated by eq. (1) over the full record length. The corresponding $^{13}C/^{12}C$ data (Fig. 1b) also shows a trend in the MLO–SPO difference, but the trend is not well constrained by $\delta^{13}C$ data alone due to the shorter record and scatter in the data, especially before newer instrumentation was used beginning in 1991. The $^{13}C/^{12}C$ data are nevertheless consistent to within the uncertainties with the trend predicted by eq. (2), using ΔC_i(ff) estimated from eq. (1).

None of the regressions for other stations, paired with the SPO records, produce results as convincing as for MLO, mainly because the records are shorter or broken, and exhibit greater scatter. Also, as will be discussed below, regressions for some stations appear to be inconsistent with those for the other stations, even allowing for uncertainty in the data. Regression results for all stations are summarized in Table 3.

Nevertheless, computed latitudinal gradients over time of ΔC_i(fit) and $\Delta\delta_i$(fit) and of ΔC_i(res) and $\Delta\delta_i$(res) contributed by all stations of our study (Fig. 2) clearly show a progressive buildup of CO_2 in the Northern Hemisphere. Early in the record period, ΔC_i(fit) shows a nearly symmetrical gradient with a peak in the tropics (cf. Bolin and Keeling, 1963). In subsequent years, an ever-increasing gradient in the north replaces this pattern. The gradients for $\Delta\delta_i$(fit) (with lower ratios plotted upwards) are similar to those for ΔC_i(fit) except that no tropical peak in $-\Delta\delta_i$(fit) is present.

The similarity of the patterns in ΔC_i(fit) and $\Delta\delta_i$(fit) north of the Equator is a strong indication that the buildup in the

Table 2. Glossary of terms and descriptors

Terms used in regressions, eqs. 1 and 2	
ΔC_i(fit)	Predicted CO_2 concentration difference of station *i* to South Pole, obtained by regression from eq. 1
ff	Global fossil fuel emissions in PgC yr^{-1}
S_i	Slope function in ppm/(PgC yr^{-1})
ΔC_i(res)	Time-invariant constant that reflects the stationary component of the CO_2 gradient
ΔC_i(ff)	$S_i \times$ ff
$\Delta\delta_i$(fit)	Predicted isotopic ratio difference of station *i* to South Pole, obtained by fit from eq. 2
δ_o and C_o	Time-varying reduced isotopic ratio and CO_2 concentration, respectively, at the South Pole
ε_{ff}	Time-varying reduced isotopic ratio of fossil fuel from Andres et al. (1996a)
$\Delta\delta_i$(res)	Time-invariant constant that reflects the stationary component of the $\delta^{13}C$ gradient
Additional terms used in the text	
ΔC_i(TM2fos)	CO_2 concentration difference of station i to SPO owing to the fossil fuel source alone, as predicted by the TM2 transport model
F_{inter}	Net annual oceanic interhemispheric carbon flux
Descriptors for inverse calculations, described in Table 5	
STND_INV	Standard inverse calculation (using adjusted data at PTB and NZD)
ORGD_INV	Inverse calculation with unadjusted data
ADJB_INV	Inverse calculation with adjusted data at PTB
FOS2_INV	Inverse calculation with TM2 model response for fossil fuel emissions replaced by the regression-determined fossil fuel value, ΔC_i(ff), at all stations
FOS3_INV	Inverse calculation with TM2 model response for fossil fuel emissions scaled down by 8% to match ΔC_i(ff) at PTB
REC2_INV	Inverse calculation with SBE component replaced by predictions from the CSU atmospheric model
ATL2_INV	Inverse calculation without the prescribed North Atlantic sink (ATL)
Descriptors for model source components, described in Appendix 1	
FOS, EXC, OCE1, OCE2, OCE3, ATL, TDE, OSU, TDF, SBE, BSU, FER, DES, BIO1, BIO2, BIO3, BIO4	
Descriptors for station names, explained in Table 1	
ALT, PTB, LJO, MLO, KUM, CHR, SAM, KER, NZD, SPO	

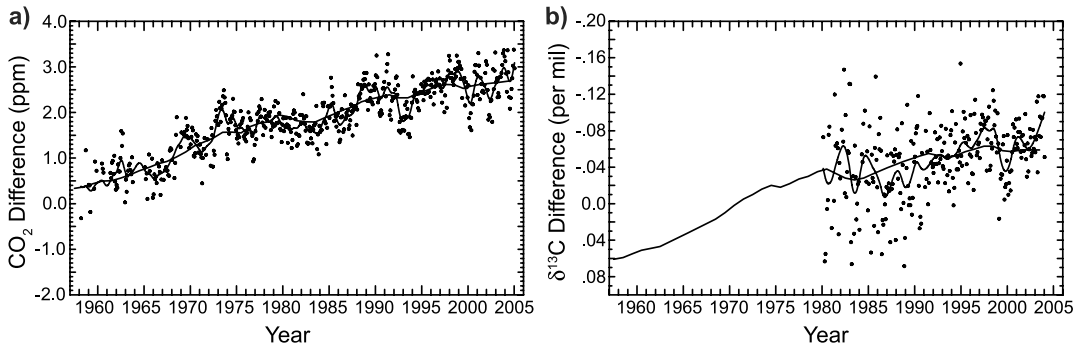

Fig. 1. Panel a: Differences versus time, in the seasonally adjusted concentration of atmospheric CO_2 between Mauna Loa, Hawaii and the South Pole, [ΔC_{MLO}(obs), monthly dots) and its linear regression on fossil fuel emissions (ΔC_{MLO}(fit), curve]. Panel b: Similar plot for the $^{13}C/^{12}C$ reduced isotopic ratio and its regression on fossil fuel emissions via eq. (2) ($\Delta\delta_{MLO}$(fit), curve). In both panels, the higher frequency curves are fits to a spline function.

gradients is due to some combination of changing fossil fuel emissions and CO_2 exchange with the terrestrial biosphere. The extent to which the terrestrial biosphere contributes, perhaps via an increasing sink, cannot be established simply by comparing the concentration and isotopic gradients, because the average $^{13}C/^{12}C$ ratio of fossil fuel and plant carbon are nearly the same, both strongly depleted in heavy carbon, ^{13}C.

The lack of a tropical peak in $-\Delta\delta_i$(fit), however, is unambiguous evidence that the concentration peak in ΔC_i(fit) is caused by an oceanic CO_2 source or a terrestrial source dominated by

Table 3. Summary of regression statistics for fits to eqs 1 and 2

	Atmospheric CO_2							Atmospheric $\delta^{13}C$			
Station[a]	Time period	Slope, *Si* (ppm/PgC y^{-1})	Sigma (ppm/PgC y^{-1})	Intercept, ΔCi (res) (ppm)	Sigma (ppm)	Correlation coefficient	Degrees of freedom	Time period	Intercept, $\Delta\delta i$ (res) (per mil)	Sigma	Degrees of freedom
PTB	1962–1964, 1966–1967, 1974–2003	0.47	0.07	0.85	0.36	0.78	33	1983–2003	−0.054	0.024	20
LJO	1958–1962, 1972–2003	0.66	0.05	−1.09	0.27	0.91	35	1979–2003	0.104	0.028	20
MLO	1959–2003	0.52	0.02	−0.84	0.11	0.96	43	1979–2003	0.132	0.015	24
KUM	1965, 1980–2003	0.54	0.07	−0.66	0.44	0.84	23	1980–2003	0.096	0.018	22
CHR	1965, 1975–2003	0.33	0.08	+0.55	0.44	0.63	28	1978–2003	0.084	0.033	25
SAM	1965, 1982–2003	0.15	0.05	+0.28	0.30	0.54	21	1984–2003	0.061	0.019	19
KER	1968, 1983–2002	0.11	0.05	−0.27	0.27	0.50	19	1984–2003	0.035	0.024	19
NZD	1962, 1968, 1978–2003	−0.01	0.04	+0.16	0.22	0.28	26	1986–2003	−0.008	0.015	17

[a]Station symbols are as explained in Table 1.

C4 plants, and not by C3 plants. To produce a tropical peak in ΔC_i(fit) but not in $-\Delta\delta_i$(fit) requires a CO_2 source that has a $^{13}C/^{12}C$ ratio similar to that of atmospheric CO_2. This requirement can only be met by a source from the oceans or from C4 plants, but not from C3 plants, which are heavily depleted in ^{13}C. The ocean influence on the $^{13}C/^{12}C$ latitudinal gradient is known to be dominated by purely isotopic exchange driven by the temperature-dependent equilibrium fractionation between the atmosphere and ocean (source component TDF in Table 2; cf. Keeling et al., 1989c, fig. 30, p. 323). As shown below in Fig. 12, this isotopic exchange process accounts very well for the stationary gradient in $\delta^{13}C$ between the South Pole and northern mid-latitudes found by the regression analysis.

4. Inverse model of latitudinal CO_2 gradient

4.1. Model description

By the regression analysis above, we have sought to distinguish aspects of the carbon cycle related to human activities [C(ff)] from undisturbed aspects [C(res)], over approximately the past 50 yr. To gain further insight into the causes of these patterns, we turn to a regional inverse model coupled with a three-dimensional atmospheric transport model (Piper et al., 2001) to establish the relationships of atmospheric CO_2 concentrations to CO_2 exchange fluxes expressed as the sum of defined model flux components. The transport model is needed to predict how local uptake and release of CO_2 by the oceans and land are modified by the three-dimensional circulation of the atmosphere, driven by specified sources and sinks of atmospheric CO_2 which separate the spatial and temporal changes in atmospheric CO_2.

For this study, we use the approach of Heimann and Keeling (1989) as modified by Piper et al. (2001) which employs the atmospheric tracer transport model TM2 (Heimann, 1995) as the basis for an inverse calculation or 'inversion'. This inverse calculation involves adjusting a series of surface source components to match optimally the atmospheric CO_2 observations, and optionally also the $^{13}C/^{12}C$ ratio. The sum of the individual source components constitutes the total flux field (note that a sink is a source in the negative sense, so both sources and sinks will often be referred to as 'sources' in this paper).

The inversion is constrained globally by a separate global single deconvolution calculation (Keeling et al., 2005), which specifies global exchange of atmospheric CO_2 with the land and oceans. In the global deconvolution, the oceanic carbon reservoir is assumed to transport carbon by vertical diffusion at a rate ($k_{\mathrm{diff}} = 7685$ m^2 yr^{-1}) that reproduces the observed uptake of radiocarbon. The net ocean CO_2 uptake is computed by driving the ocean model with the observed atmospheric CO_2 rise, and the net exchange flux with the terrestrial biosphere is computed based on the change in atmospheric CO_2 not accounted for by fossil fuel emissions and ocean uptake. The net land uptake is

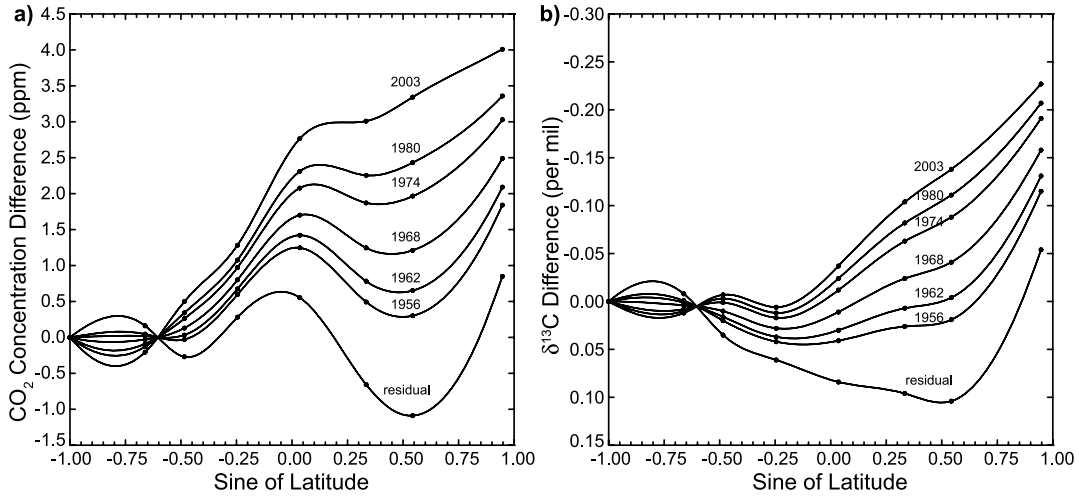

Fig. 2. Panel a: Latitudinal gradients (dots connected by smooth curves) of the regression concentration differences, ΔC_i(fit), for selected years and of the stationary difference, ΔC_i(res). Panel b: Similar plot for isotopic differences, $\Delta\delta_i$(fit) and $\Delta\delta_i$(res). Dots indicate station locations. Sine of latitude rather than latitude is used for the *x*-axis in this and following figures because it scales as surface area of the Earth.

represented as the sum of a term related to CO_2 fertilization of land photosynthesis, and a second term that includes emissions owing to land-use change. The deconvolution calculation also yields estimates of the isotopic exchange fluxes with the land and oceans, including the so-called Suess effect, or 'isoflux' terms.

In the inverse calculation, atmospheric responses for each of the source/sink components are combined linearly and adjusted in strength to achieve a best fit to the station observations of CO_2 and $^{13}C/^{12}C$. In this study, we use the same year of wind fields for all years in the simulations. For each year of simulation, we recycle the windfields for 4 yr after which the annual change in concentration in every model grid box closely approaches a constant.

The inverse model includes 17 source components (See Table 4 and Appendix B). Source component FOS varies strictly with fossil fuel emissions and is based on data from international governmental sources (Marland et al., 2005) without adjustment. Terrestrial component FER and oceanic component EXC vary closely but not strictly with fossil fuel emissions. Terrestrial component SBE allows for purely seasonal exchanges with the land biosphere. Seven zonal components, four terrestrial (BIOi) and three oceanic (OCEi), are free to vary without regard for proportionality with fossil fuel CO_2 emissions. The components, DES, ATL and TDE, set to be strictly stationary, account for exchanges driven by land-use, interhemispheric oceanic transports and seasonal exchanges with the oceans, respectively.

In addition to the above source components, which influence both atmospheric CO_2 concentration and isotopic composition in specified proportions, the inverse model includes three components that influence the isotopic composition alone: TDF, which accounts for isotopic exchange with the oceans, driven by temperature-dependent fractionation, and OSU and BSU, which account for the ocean and land biosphere ^{13}C Suess effects, respectively. The isotopic signature of all oceanic components is very small, except for the TDF component. Therefore, almost all isotopic temporal variability, which affects the model prediction of CO_2 concentration, is terrestrial in origin.

Of the 17 components, all but seven (BIOi and OCEi) have magnitudes that are prescribed a priori. The prescribed components DES, ATL and FER have little effect on the model results because error in assigning those magnitudes is mostly compensated for by the adjustable BIOi and OCEi components. DES, ATL and FER are included in the model because the spatial distributions of these fluxes, based on prior information, are prescribed differently from those of BIOi and OCEi. For simplicity, the DES term is treated here as time invariant.

Inversions were carried out for each year from 1958 to 2003 using as inputs the concentration and isotopic data, ΔC_i(fit) and $\Delta\delta_i$(fit), which are shown for selected years in Figs 2a and b, respectively. A model fit was also carried out using the stationary gradients in CO_2 and $^{13}C/^{12}C$ as the entire atmospheric signal. For the stationary fit, we set all of the prescribed time-varying components (FOS, FER, BSU, EXC and OSU) as well as component DES to zero, and we set the atmospheric CO_2 and $\delta^{13}C$ values at the South Pole to the preindustrial values of 276.91 ppm and −6.370 per mil, respectively.

The model predictions do not perfectly match the observations because the fits are over constrained, with seven unknowns (BIO1–4, OCE1–3) and 18 observations (CO_2 and $\delta^{13}C$ for eight station-pairs, and two global total net fluxes, one each for ocean and terrestrial biosphere) (cf. Fig. 3a for δ13C). The inverse calculation results nevertheless agree well with the input data at all stations, for years 1958–2003, and also agree well with the stationary component. For year 2003, the combination of all the land components yields a 1.5 Pg yr^{-1} sink in the Northern temperate zone which is offset by 1.4 Pg yr^{-1} source in the

Table 4. Model source components

		Prescribed time evolving	Prescribed stationary	Adjustable
Fossil fuel (industrial) source components				
FOS	Emissions from fossil fuel combustion and cement production	X		
Terrestrial biospheric source components				
SBE	Seasonal biosphere exchange[b,c]		X	
FER	Stimulated plant growth	X		
DES	CO_2 release from land use change		X	
BSU	Land biospheric $^{13}C/^{12}C$ Suess effect[a]	X		
BIOi (i = 1,2,3,4)	Zonal land biospheric fluxes			X
Oceanic source components				
EXC	Sink in response to fossil fuel emissions	X		
TDE	Variable temperature-dependent exchange[b,c]		X	
ATL	Atlantic sink balanced by southern source[b]		X	
OSU	Oceanic $^{13}C/^{12}C$ Suess effect[a]	X		
TDF	Temperature-dependent fractionation[a,b]		X	
OCEi (i = 1,2,3)	Zonal ocean fluxes			X

[a]Isotopic flux only; all other sources comprise a CO_2 flux as well.
[b]Source prescribed with zero net flux globally.
[c]Source prescribed with zero net CO_2 flux at each grid box but with imbalances in isotopic exchange driven by changing atmospheric $\delta^{13}C$ (terrestrial Suess effect).

tropics, with small terrestrial fluxes elsewhere. The corresponding combination of ocean components for year 2003 requires a sink everywhere except the tropics. These fluxes are generally in the range of other recent estimates (e.g. Gloor et al., 2003).

For the stationary component, the combination of land components requires biospheric sources of 3.1 PgC yr^{-1} in the northern boreal zone and 1.4 PgC yr^{-1} in the southern subtropical zone, offset by biospheric sinks in the other zones. The need for these large fluxes can be understood with reference to the stationary component of the isotopic profile shown in Fig. 3a. The large boreal emissions are required by the high values for the stationary components of CO_2 and $-\delta^{13}C$ at Barrow (PTB) relative to the other stations in the Northern Hemisphere, as shown in Fig. 3a for $-\delta^{13}C$. The large fluxes in the tropics and the Southern Hemisphere are influenced by the sharp gradient in the stationary $\delta^{13}C$ value between Kermadec (KER) and New Zealand (NZD). This gradient, owing to strong curvature, implies a strong stationary terrestrial source south of NZD at 41°S coupled to a strong terrestrial sink near KER (29° S) which require unreasonably large opposing fluxes to exist where land areas are too small for this to be possible. The calculation for year 1960 near the beginning of the observations has nearly as large land fluxes.

4.2. Model sensitivity to data from individual stations

It is not easy to reconcile the large stationary land fluxes found by the inversions with the expected behaviour of the carbon cycle. In steady-state, the oceans can be a sink of carbon in one region and a source in another, balanced by transport of carbon in the ocean's interior. In contrast, the land biosphere can only be a net source or sink (except for a small contribution due to river transports), as the result of a non–steady-state process, such as climate changes or other disturbances, human or natural. The inversion results for the stationary gradient are therefore questionable, as they indicate that large land fluxes have persisted over the past 50 yr that are unrelated to recent human activities. These fluxes are evidently tied to questionable regression results from PTB and NZD, so it is pertinent to ask whether an alternative fit without such large non–steady-state land fluxes can be obtained within the uncertainties of the regressions (e.g. via eqs (1) and (2)) to these two stations.

Figure 3a also shows not only the full inverse calculation for the stationary $\delta^{13}C$ gradient (solid curve), but also the sum of contributions to this calculation from steady-state processes (long-dashed curve), thereby excluding the non–steady-state land components (BIO1–4). In fact, the sum of the steady-state components yields a curve that is in good agreement with the regression results at all stations except those two already highlighted: at PTB there is a large discrepancy of 0.13 per mil, and at NZD, a smaller discrepancy of 0.03 per mil.

For NZD, the data records are relatively broken with considerable scatter, so the steady-state model values for CO_2 and $\delta^{13}C$ are within the uncertainty in the fit. The fit at PTB is not so imprecise, but we have evidence from measurements obtained from

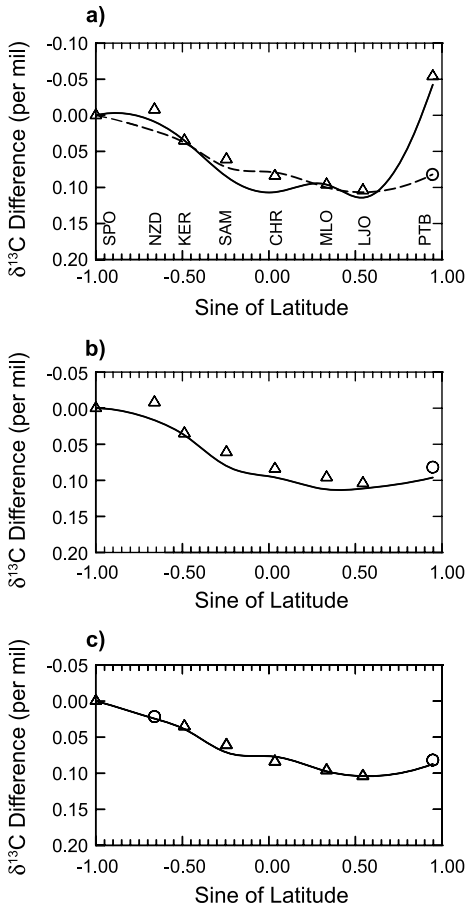

Fig. 3. Stationary component of the interhemispheric gradients in δ^{13}C based on data regressions (open triangles) compared with model fits to these data based on inverse calculations (solid curves). All curves and data points normalized to zero at the South Pole. Results from adjusted regressions shown by open circles (see text). Panel a: Comparison without any adjustments to regressions, ORGD_INV calculation (see Table 5) (solid curve) and contributions from steady-state processes only (dashed curve). For explanation of station abbreviations, see Table 1. Panel b: Comparison using adjusted data at Barrow, ADJB_INV calculation. Panel c: Comparison using adjusted data at both Barrow and New Zealand, STND_INV calculation. Results for inverse calculations are mathematically interpolated between station points.

two ice floes in the Arctic Ocean basin during the IGY that the steady-state model values are equally plausible. These ice-floe data, averaged for the two Arctic sites, which were taken on the same days as measurements at the South Pole in 1957 and 1958, are plotted in Fig. 4. Taking account of these data, an additional regression for CO_2 concentration was carried out, forced to fit the difference between the ice floe and SPO data (Fig. 5). Although the adjusted regression produces a poorer fit to the PTB data than the original regression and is especially poor for the early PTB data from 1961 to 1967, it is not clear that the PTB data produce a reliable extrapolation by themselves. Data were obtained from a site directly on the shore of the Arctic Ocean in 1961–1963, and from a site 2 km inland from 1965–1967, before the current site was established inland and farther east in 1974. What may have caused these discrepancies cannot be determined without at least obtaining new data for the first two sites and comparing it with the present site. In any case, the stationary difference ($\Delta C_{\rm PTB}$(res)) obtained for the new regression is −1.36 ppm, which agrees remarkably well with the steady-state model prediction of −1.32 ppm.

To investigate the sensitivity of the model to input data from PTB and NZD, we perform two alternative inverse calculations. In the first, we replace the input PTB data with CO_2 and δ^{13}C values predicted by the model when the non–steady-state components are excluded. In the second, we make the same replacement at PTB and a similar replacement at NZD. The steady-state model-predicted replacement values are shown by open circles in Figs 3b and c. As shown in Fig. 3b, when the model fit is repeated using the adjusted PTB points, the agreement between the model fit and observations for the stationary gradient is improved not only at PTB, but also at lower latitudes. This adjustment reduces the large land source in the boreal zone and reduces the compensating land sinks in the tropics and northern temperate zone.

As shown in Fig. 3c, when the model fit is repeated using adjusted points for NZD in addition to PTB, the agreement between model fit and observations is improved not only at NZD but also at lower latitudes. This adjustment reduces the large land source in the southern and reduces the compensating land sinks in the tropics.

In the analysis that follows, we adopt the revised model fit with adjusted points for PTB and NZD (Fig. 3c), as our preferred standard inverse calculation, abbreviated STND_INV. (The full suite of inverse calculation descriptors and abbreviations used in this paper are listed in Table 5). The STND_INV calculation yields much smaller land biospheric fluxes for the stationary gradient than either the calculation with unadjusted data (ORGD_INV calculation) or with Barrow data adjusted only (ADJB_INV calculation), as discussed further below. We also examine the sensitivity of results to different assumptions about the stationary values, as a means to explore the uncertainties.

5. Data and model-based decomposition

The foregoing analysis allows us to decompose the contemporary interhemispheric gradient into a series of different components. First, the regression analysis partitions the smoothed contemporary gradient, ΔC_i(fit), into a stationary part, ΔC_i(res) and a part that co-varies with fossil fuel emissions, ΔC_i(ff). In Fig. 6, we show this partitioning for 2003, the last year of analysis. The gradients for earlier years (not shown) are similar, except that ΔC_i(ff) is smaller, in proportion with fossil fuel, and ΔC_i(fit), the sum of ΔC_i(ff) and ΔC_i(res), reflects the change

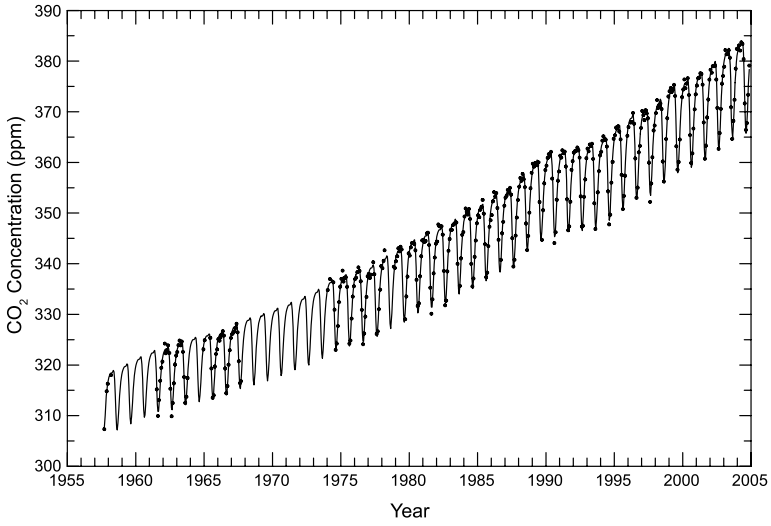

Fig. 4. The CO_2 concentration, in ppm, versus time, from observations for Arctic ice floes, 1957–1958, and Point Barrow, Alaska, 1961–1968 and 1974–2003, shown as monthly averages (dots) and a spline fit combined with seasonal harmonics increasing in amplitude at an assumed constant rate (smooth curve).

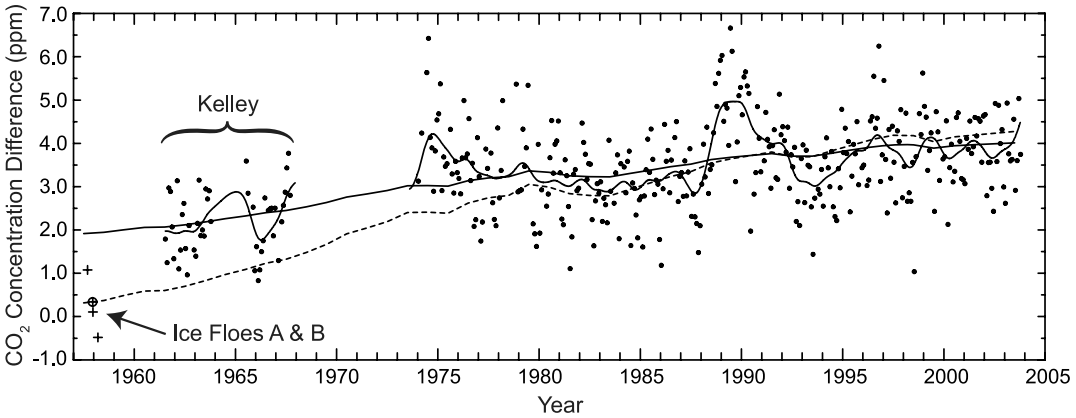

Fig. 5. Regression plot, similar to Fig. 1, but for Barrow data, including in situ data from 1961–1967 reported by Kelley (1969) and flask data from 1974–2003 from the Scripps CO_2 Program. Also shown are data from ice floes A and B (1957–1958). Stiff solid curve: regression to Barrow data (1961–2003). Stiff dashed curve: regression to flask data from Barrow (1978–2003) and ice floes. The higher frequency curves are fits to a spline function. The Kelley data are used with corrections including for the carrier gas effect.

Table 5. Inverse calculations

Calculation descriptor and abbreviation	Input data for regressions	Model source components
Standard (STND_INV)	Base case[a]	Unmodified[b]
Original data (ORGD_INV)	Original data	Unmodified
Adjusted Barrow data (ADJB_INV)	Adjusted PTB	Unmodified
FOS from regression (FOS2_INV)	Base case	FOS from regression
FOS rescaled (FOS3_INV)	Base case	FOS rescaled from TM2 to match the adjusted PTB-SPO regression
Alternate rectifier (REC2_INV)	Base case	SBE based on Denning et al. (1995)
ATL component excluded (ATL2_INV)	Base case	ATL component excluded

[a]Used adjusted regressions at both PTB and NZD.
[b]Model components as described in Appendix B using TM2 transport model.

in ΔC_i(ff). All of these parameters are entirely data-based and model-independent.

Second, we separate the co-varying component of the gradient into a part that is directly caused by fossil fuel emissions, plus a component, which has evolved over time similarly to fossil fuel emissions but is caused by other CO_2 sources and sinks. This additional time-evolving component can be estimated as the difference ΔC_i(TM2fos)–ΔC_i(ff), where ΔC_i(TM2fos) is the

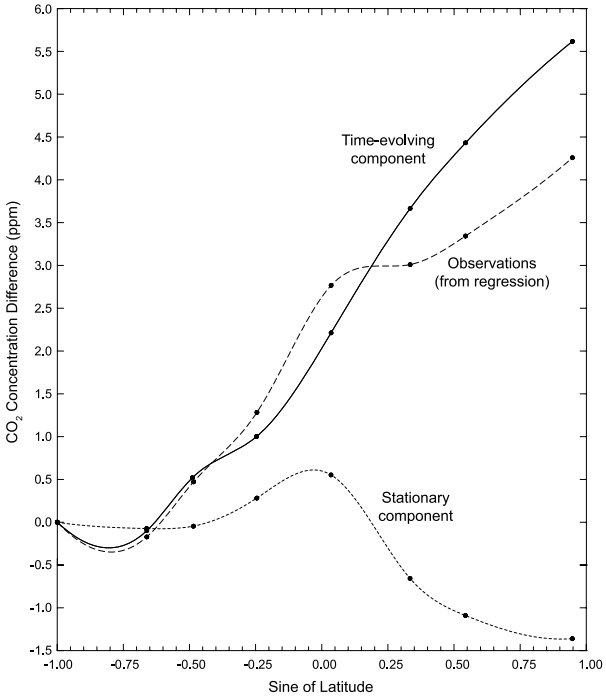

Fig. 6. Latitudinal gradients of CO_2 regression terms for 2003: observations from regression [ΔC_i(fit)]; time-evolving component tied to fossil fuel emissions [ΔC_i(ff)] and the stationary component [ΔC_i(res)].

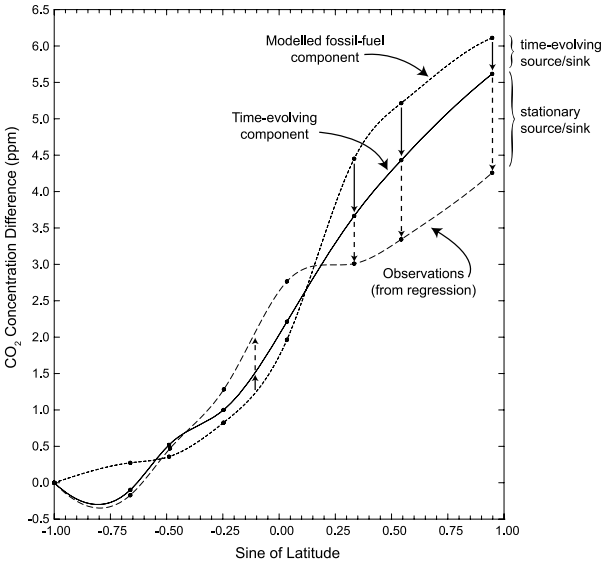

Fig. 7. Comparison of latitudinal gradients of atmospheric CO_2 for 2003: prediction of observations by regression [ΔC_i(fit)]; modelled contribution from fossil fuel emissions using the TM2 model [ΔC_i(TM2fos)] and time-evolving component tied to fossil fuel emissions [ΔC_i(ff)].

response to fossil fuel alone as predicted by the TM2 transport model. As shown in Fig. 7, the latitudinal gradient of ΔC_i(ff) has a smaller gradient from the Arctic to the South Pole than expected for fossil fuel emissions alone, with a distinctly less-steep descent in the tropics. The observed gradient ΔC_i(fit), in turn, is even less steep than ΔC_i(ff). Thus the time-evolving and stationary components both contribute to the reduction in the interhemispheric gradient, with about 30% of the reduction in the gradient (as measured from PTB to SPO) being due to the time-evolving component and the remainder due to the stationary component, according to this analysis.

Third, using the standard inverse calculation, STND_INV, we further resolve the time-evolving and stationary components of the gradients into separate land and ocean components, as shown in Fig. 8. The fluxes contributing to these gradient components, averaged over coarse latitude bands, are shown in Fig. 9.

The land contribution to the time-evolving fluxes consists of a sink in 2003 of 1.7 PgC yr^{-1} in the northern temperate zone (23.5–47°N), which is nearly but not completely offset by a source of 1.2 PgC yr^{-1} in the tropics plus small sources in other zones. These land biospheric fluxes contribute 1.3 ppm to the reduction in the interhemispheric gradient (PTB-SPO) (Fig. 8a). The ocean contribution to the time-evolving component is essentially given by the perturbation ocean sink component (EXC) because the other ocean components, which are allowed to freely vary in the inversion, are found to be nearly constant with time, as discussed earlier. The perturbation ocean sink increases the interhemispheric gradient (PTB-SPO) by 0.8 ppm, partially offsetting the contribution from land biospheric exchanges.

The land contribution to the stationary gradient is very small (Fig. 8b). The annually balanced, seasonal biospheric exchanges (SBE) contribute to the gradient by 0.1 ppm, via the so-called seasonal rectifier effect. Annually imbalanced (i.e. 'net') exchanges with the land biosphere make only a small contribution (−0.1 ppm) to the interhemispheric gradient (PTB-SPO). The ocean contribution consists of a source of 1.4 PgC yr^{-1} in the tropics, which is largely balanced by uptake of 1.2 PgC yr^{-1} in the northern extra-tropics, with the fluxes in the southern extra-tropics being much smaller. These ocean fluxes contribute to the reduction of the interhemispheric gradient (PTB-SPO) by 1.3 ppm (Fig. 8b).

6. Further model sensitivities

We now extend the sensitivity analysis of the model to include not just alternate assumptions about the data, but also assumptions about prescribed model components, including sensitivity to the dispersal of fossil fuel CO_2, the seasonal rectifier effect and assumptions regarding ocean transport. The full suite of inverse model calculations is summarized in Table 5, with the impact of different assumptions on the stationary and time-varying ocean and land fluxes summarized in Figs 10 and 11.

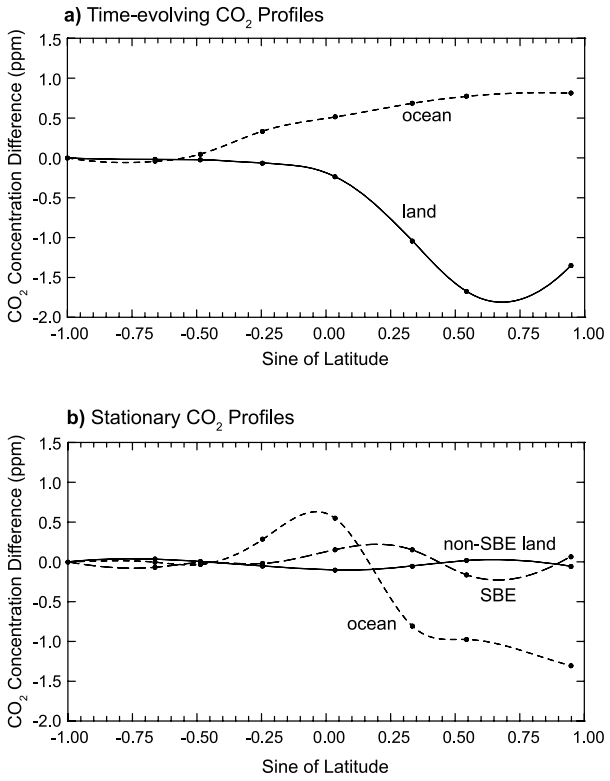

Fig. 8. Components of the interhemispheric gradient for 'Standard' inverse calculation, STND_INV (see Table 5). Panel a: Time-evolving oceanic (dash) and land biospheric (solid) components for 2003. Panel b: Stationary oceanic (short dash) and land biospheric components, with seasonal biospheric exchange (SBE) (long dash) shown separately from the other land biospheric components (solid).

6.1. Sensitivity to dispersal of fossil fuel CO_2

In a comparison of 12 transport models in the TRANSCOM project (Law et al., 1996), the TM2 prediction of the zonal annual-mean surface atmospheric CO_2 concentration for the fossil fuel source fell near the middle of predictions by all models; however, the TM2 version used in this study has a coarser grid (8×10 degrees in the horizontal, with nine vertical layers) than the version used in TRANSCOM (4×5 degrees by 16 vertical layers), and predicts a latitudinal gradient about 0.6 ppm larger for the 5.3 PgC yr^{-1} source, near the upper limit of TRANSCOM model predictions. As is clear from Fig. 7, if the gradient predicted by TM2 were reduced by 0.6 ppm, it would largely agree with the component tied to fossil fuel found by regression, eliminating the need for a time-evolving source-sink component.

To further explore the sensitivity of the results to the dispersal of fossil fuel CO_2, we carried out two additional model fits: (1) we replaced the TM2 model response for fossil fuel emissions by the regression-determined fossil fuel value, ΔC_i(ff), at all stations, while still adopting the TM2 predictions for the other source components; in other words, we assumed in this case that ΔC_i(ff) represents exclusively the atmospheric response to fossil fuel emissions (FOS2_INV calculation), and (2) we scaled downwards the TM2 model response at all stations by 8% as required to match ΔC_i(ff) at Point Barrow alone (FOS3_INV calculation).

As shown for the FOS2_INV calculation in Fig. 11, this change has relatively little impact on the ocean fluxes, but almost completely eliminates the need for a time-varying land biospheric sink in the northern temperate zone, and changes the tropical biospheric flux from a source of 1.7 PgC yr^{-1} to a small sink of 0.2 PgC yr^{-1} (corresponding total fluxes for 2003 of a 1.2 PgC yr^{-1} source and 0.7 PgC yr^{-1} sink are obtained by adding in the stationary fluxes of Fig. 10).

For the FOS3_INV calculation, shown in Fig. 11, the ocean fluxes again change little, and the northern temperate and tropical fluxes change a much smaller amount than in the first case, decreasing on order of the percentage decrease applied to the TM2 model response (8% decrease in the TM2 model response, 11% reduction in northern temperate sink, 13 % reduction in tropical source). These results indicate that the inverse fluxes are quite sensitive to fine details of how fossil fuel CO_2 is dispersed, and not sensitive merely to the overall latitudinal gradient induced by fossil fuel burning.

6.2. Sensitivity to the rectifier component

The covariation of seasonal atmospheric transport with SBE can lead to a gradient in annual mean CO_2. This process is known as the seasonal rectifier effect and is depicted in our inverse model via the SBE component. Transport models with seasonally varying boundary layer heights, such as the Colorado State University (CSU) model (Denning et al., 1995), tend to produce substantially larger latitudinal gradients in mean annual CO_2 than do models, such as TM2 used in this study, that have time-invariant boundary layers. To explore the sensitivity of our results to the assumed magnitude of the seasonal rectifier, we performed an additional inverse calculation, REC2_INV calculation, in which we replaced the SBE component with predictions from the CSU model. All other inputs to the calculation were the same as in the STND_INV calculation.

The rectifier effect also influences the interpretation of the stationary component of the δ^{13}C gradient. As shown in Fig. 12a, the stationary δ^{13}C gradient is fit equally well using either the TM2 or CSU estimate of the rectifier. The fit is achieved largely on the basis of a single oceanic component, temperature-dependent fractionation between air and sea (TDF), which matches the stationary δ^{13}C gradient very well by itself (Fig. 12b). The various land contributions to the stationary δ^{13}C gradient must therefore largely cancel. Because the CSU rectifier produces, by itself, a large gradient in δ^{13}C, as shown in Fig. 12c, the cancellation is achieved with the CSU rectifier by requiring large stationary fluxes on land that oppose this gradient. The pattern is dominated by a boreal sink of $\sim$1.7 PgC yr^{-1} offset

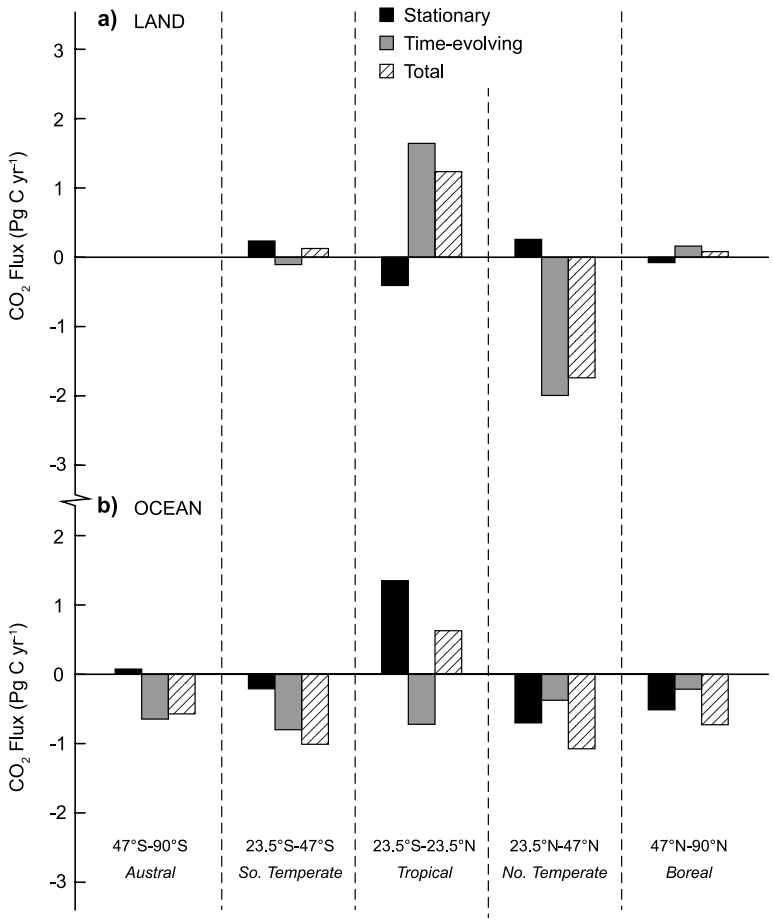

Fig. 9. Zonal fluxes, in PgC yr^{-1}, from the 'Standard' inverse calculation, STND_INV, shown for 2003 separated into stationary and time-evolving fluxes. Panels a and b show land and ocean fluxes respectively.

by a tropical source, as shown in Fig. 10. In contrast, the TM2 rectifier produces, by itself, almost no gradient, so the required stationary land fluxes are very small.

If the large CSU rectifier is correct, these findings imply the existence of a persistent large northern biospheric sink coupled with a large tropical source, assuming that $\Delta\delta_i$(res) are accurate estimates of the stationary component of the δ^{13}C gradient. Integrated over the period of analysis, from 1958 to 2003, the cumulative northern sink would amount to 46 PgC.

6.3. Sensitivity to ocean transport

The STND_INV calculation prescribes a North Atlantic ocean sink of 0.7 PgC yr^{-1}, coupled with a southern ocean source of the same magnitude, following Piper et al. (2001). Recent work by Mikaloff Fletcher et al. (2007) employing an inverse method and ocean interior observations supports a lower estimate of 0.3 PgC yr^{-1}, at the low end of the range of previous estimates that we considered in making our prescription (see Appendix B).

It is possible that this prescription biases high our inverse estimate of the northern ocean sink. We tested this possibility by repeating the inverse calculation without this source component included (ATL2_INV calculation). As shown in Fig. 10, zonal fluxes produced by the ATL2_INV calculation differ from those of the STND_INV calculation by less than 0.16 PgC yr^{-1} in all zones. Evidently, the zonal oceanic sources included in the model (OCE1–3), which are distributed over all oceans, readily compensate for changes in the prescribed North Atlantic sink component.

7. Summary and discussion

7.1. Observed gradients

We have examined the interhemispheric gradient in atmospheric CO_2 and its evolution over time in the context of the longest existing records of CO_2 concentration and isotopic composition. Consistent with prior studies, our analysis documents the progressive buildup of a CO_2 excess in the Northern Hemisphere tied to fossil fuel burning, a buildup which appears to be superimposed on a non-zero background or 'stationary' gradient. The stationary CO_2 gradient has a maximum at stations in the

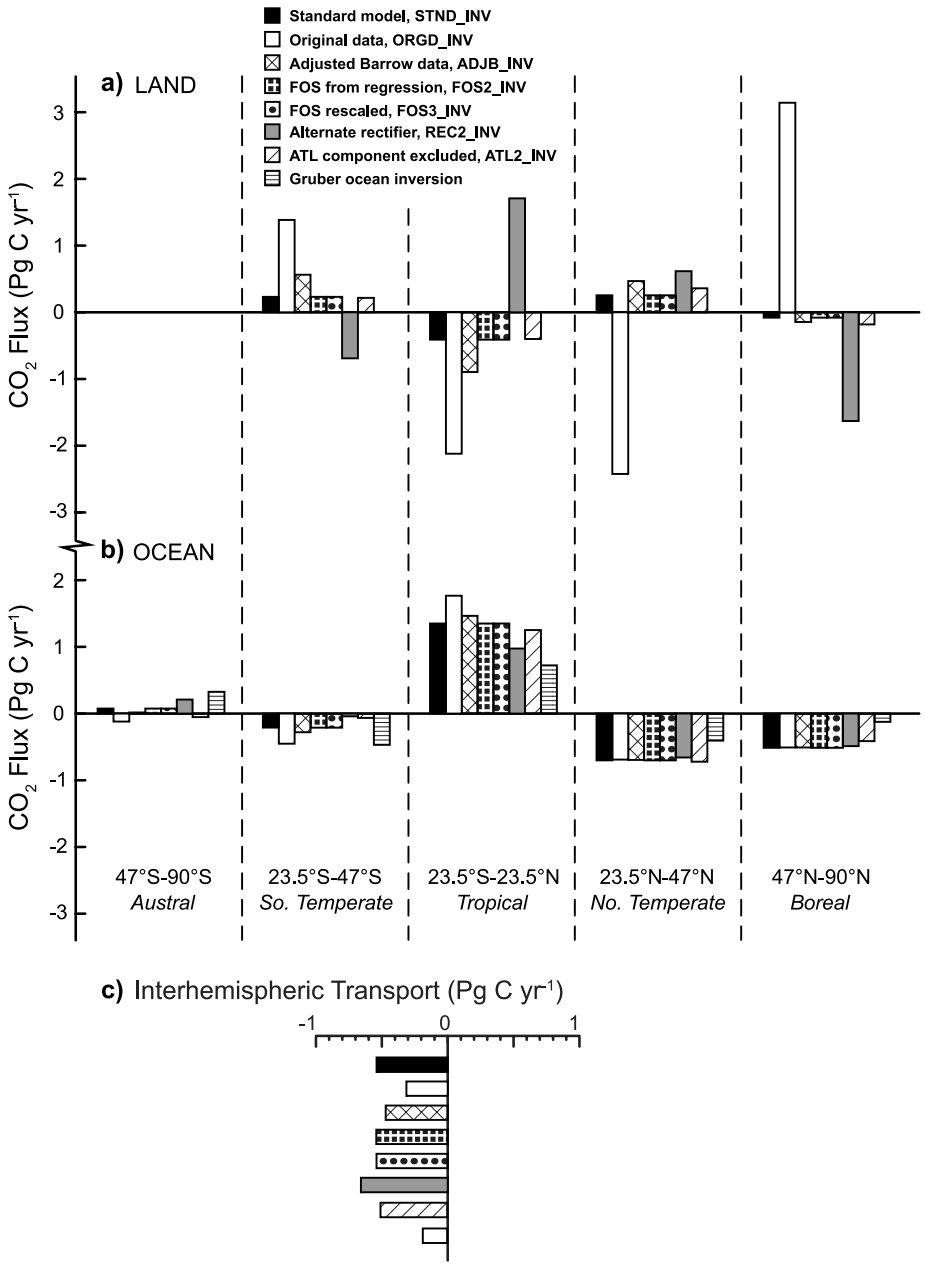

Fig. 10. Stationary fluxes, in PgC yr^{-1}, for the inverse calculations summarized in Table 5. Panel a shows land fluxes and Panel b shows ocean fluxes. Panel c shows the interhemispheric oceanic transport of CO_2 for each case; negative fluxes are southwards, as defined in Section 7.2. The fluxes labelled 'Gruber ocean inversion' are averages for ocean inversions reported by Gruber et al. (2009) based on the study of Mikaloff Fletcher et al. (2007). The natural fluxes reported by Gruber et al. (2009) were redistributed to our zones using the detailed region descriptions from Mikaloff Fletcher et al. (2003).

tropics with concentrations in the northern extratropics generally being around 1 ppm lower than the southern extratropics. An exception to this pattern is at Barrow, Alaska, but here the data appear inconsistent with independent measures of arctic CO_2 levels in the 1950s based on samples obtained on Arctic ice floes.

Our analysis also documents an evolving gradient in $\delta^{13}C$ of CO_2 due to fossil fuel burning. By combining the $\delta^{13}C$ data with CO_2 data, we also resolve this evolving $\delta^{13}C$ gradient into a component tied to fossil fuel burning and a stationary component. Except for Barrow, this stationary $\delta^{13}C$ gradient generally has higher $\delta^{13}C$ values in the north and south. The anomalous

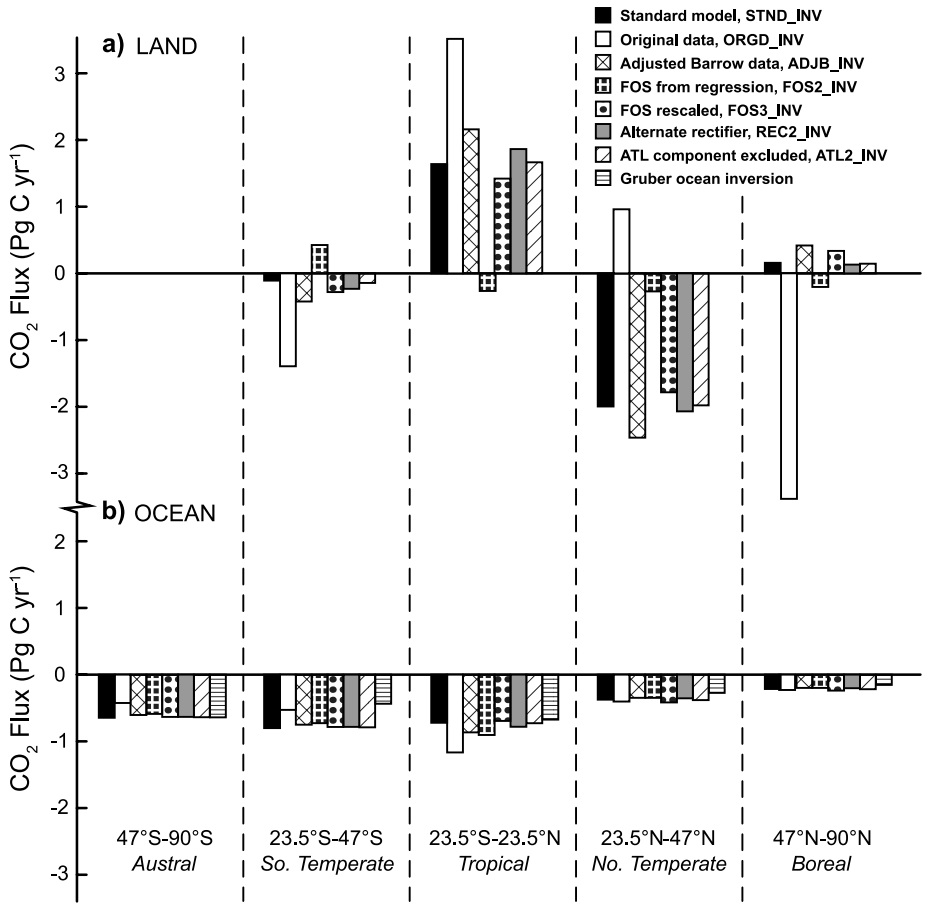

Fig. 11. Time-evolving fluxes, in PgC yr^{-1}, in 2003, for inverse calculations summarized in Table 5, and for the Gruber Ocean inversion as described in Fig. 10.

δ^{13}C value at Barrow is tied to the anomalous CO_2 value, and is therefore questionable based on the ice floe data.

7.2. Ocean contribution to gradient

Using the TM2 atmospheric transport model, we have shown that the stationary δ^{13}C gradient (after making adjustments at Barrow) can be adequately explained based on a single process—temperature-dependent fractionation between air and sea—which requires that the stationary CO_2 gradient be driven by other processes that have little influence on δ^{13}C, such as oceanic processes or exchange with C4 plants. Although data uncertainties prevent us from firmly excluding a contribution from C3 plants to the stationary gradients in CO_2 and δ^{13}C, oceanic exchanges appear able to fully account for these gradients to within the observational uncertainties. In this analysis, air-sea exchanges account for the tropical maximum in the stationary CO_2 gradient, as well as the deficit in the north compared to the south.

The notion that natural air–sea exchanges cause a tropical maximum in atmospheric CO_2 is highly consistent with a wide body of work, dating back to Bolin and Keeling (1963), who attributed this feature to upwelling-driven outgassing of CO_2 along the Equator and ingassing to the north and south. This natural pattern of air–sea CO_2 exchange is now characterized by extensive observations of the pCO_2 distribution in surface waters (Takahashi et al., 2002).

The notion that natural air–sea exchanges contribute to a background interhemispheric CO_2 gradient of order 1 ppm has been more controversial, however. A 1 ppm gradient likely requires a natural southward transport within the ocean of around 0.5 PgC yr^{-1} from one hemisphere to the other, balanced in steady-state by a northward return flux in the atmosphere (Fan et al., 1999). Similar to the study of Keeling et al. (1989c), our results require greater southward transport than found in other recent studies. But before comparing with these studies, we first address the question of how best to report interhemispheric ocean transport.

The net carbon flux across the Equator is the most obvious measure of interhemispheric transport. However, this measure is clearly problematic in the present context because the flux at precisely the 0° latitude depends on fine details of the

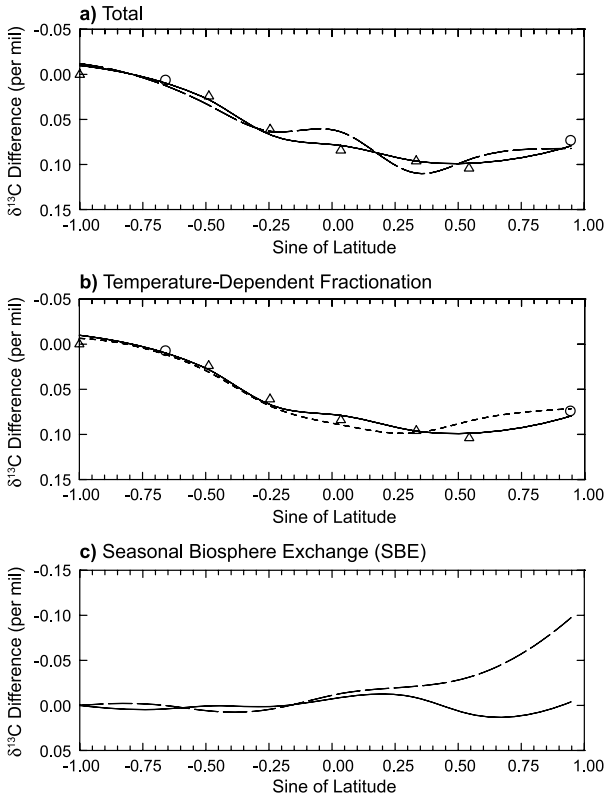

Fig. 12. Panel a: Stationary component of the interhemispheric gradient in δ^{13}C based on 'base case' regressions (open triangles and circles, see Table 5) compared with the STND_INV (solid curve) and REC2_INV (dashed curve) inverse calculations. Panel b: Contribution from temperature-dependent fractionation to δ^{13}C gradient (short dashed curve) versus regression and STND_INV calculation results (same as in Panel a). Panel c: Comparison of the rectifier components used in the STND_INV (solid curve) and REC2_INV (dashed curve) inverse calculations. In the REC2_INV calculation, the rectifier effect on the total latitudinal gradient is largely offset by a land sink in the north.

tropical ocean circulation that have negligible influence on the atmospheric interhemispheric gradient. Atmospheric inversions, for example, cannot resolve the equatorial outgassing into separate northern and southern components. While recognizing this limitation, most studies have nevertheless used the flux across the Equator as the reported measure (Fan et al., 1999; Gloor et al., 2003; Mikaloff Fletcher et al., 2007).

A more appropriate measure, we suggest, is the average flux across a symmetric pair of latitudes that are far enough from the Equator to be insensitive to the equatorial outgassing. Thus here we take $F_{\text{inter}} = (F_{\text{N}} + F_{\text{S}})/2$, where F_{N} is the net northward transport in the ocean interior across 23.5°N whereas F_{S} equals the net northward transport across 23.5S. In steady-state F_{N} equals the integrated sea to air flux north of 23.5°N and $-F_{\text{S}}$ is the integrated sea to air flux south of 23.5°S. F_{inter} can be viewed as an interpolated estimate of the flux across the Equator. However in contrast to the flux across the Equator, F_{inter} depends only on steady-state air–sea fluxes in the extratropics. These extratropical fluxes clearly have leverage to influence the atmospheric interhemispheric gradient and therefore can be constrained with the atmospheric data. Because F_{inter} excludes the large fluxes in the tropics, we expect that its value is not highly sensitive to the arbitrary reference latitudes of 23.5°.

The estimates of F_{inter} for our different inverse calculations are shown in the bottom panel of Fig. 10. Discounting the inverse calculation using the original data from PTB (ORGD_INV calculation), which we expect leads to erroneous results, all calculations require a steady-state southward ocean transport of between 0.47 and 0.67 PgC yr^{-1}. In comparison, Keeling et al. (1989c) report a steady-state southward cross-Equator flux of 0.94 PgC yr^{-1} (based on analysis of atmospheric data in 1962) but this must be reduced by 0.22 PgC yr^{-1} to account for asymmetries that they prescribed in the Equatorial outgassing. The corrected figure of 0.72 PgC yr^{-1} (referenced to 16° latitude) is in good agreement with the new fits reported here. Similar estimates were found by Keeling et al. (1989c) for other time periods (see their table 10) and a similar estimate was reported in the earlier study of Keeling and Heimann (1986) using similar methods and data. In both of these earlier studies, the interhemispheric transport was attributed to the Atlantic overturning circulation, and rationalized based on the higher carbon content of the southward-flowing North Atlantic Deep Water as compared to the shallower return flow. In our analysis, we allow the transport to be carried by a combination of fluxes from all oceans.

Our estimate of ocean interhemispheric transport can be compared to recent estimates based on ocean inversion studies and forward ocean model simulations (Mikaloff Fletcher et al., 2007; Gruber et al., 2009). Taking the values reported in Mikaloff Fletcher et al. to compute F_{inter} (referenced to 18°N and 18°S) yields estimates of southward transport ranging from −0.17 to −0.23 PgC yr^{-1} depending on the model and approach. The average for these values reported by Gruber et al. (2009) is shown in Fig. 10. The southward transport is considerably smaller than our estimates and those of Keeling et al. (1989c) and Keeling and Heimann (1986). The discrepancy may result in part from our using a very sparse network of stations and rather 'stiff' (i.e. broad regional) basis functions. Allowing for more flexibility in the source/sinks patterns could conceivably allow for a smaller (or larger) interhemispheric flux by the oceans.

It also seems possible that the ocean inversion and ocean model studies may underestimate the southward transport. Doney et al. (2004) have shown that the low-resolution ocean models typically used in carbon studies (Gloor et al., 2003; Jacobson et al., 2007) typically underestimate the northward transport of heat in the Northern Hemisphere and overestimate the southward transport of heat in the Southern Hemisphere, such that transport of heat is too symmetric about the Equator as compared to observations. The errors can be traced in part to Atlantic overturning circulation in the models, which tends

to be too weak and too shallow. Heat flux errors of this sense would also be expected to lead to an underestimate of the southward CO_2 transport by the oceans when the models are used to simulate CO_2 transports.

It is also possible that the Pacific and Indian Oceans make a significant contribution to the interhemispheric transport. The deep circulation of these oceans is highly asymmetric, with waters deeper than ~900 m (density anomaly $\sigma = 27.3$) outcropping to the surface in the Southern Hemisphere but not in the Northern Hemisphere (Robbins and Bryden, 1994). Carbon which is exported into the deep ocean via sinking particles, whether in the North Pacific, South Pacific, Equatorial Pacific or Indian Oceans is thus returned to the surface as dissolved inorganic carbon principally at high southern latitudes. This asymmetry in the deepwater circulation therefore has the potential to support a carbon 'loop' in which CO_2 is removed from the atmosphere by marine photosynthesis and air–sea exchange in the Equatorial and North Pacific and Indian Oceans, and returned to the atmosphere at high southern latitudes. A significant North Pacific CO_2 uptake has been found in the modelling study of Doney et al. (2006) qualitatively consistent with the operation of this loop. A pre-industrial North Pacific CO_2 sink in the 36°N–49°N band is also supported by the hydrographic data in the North Pacific (Jacobson et al., 2007, Fig. 3, bottom panel).

Present models may have a tendency to underestimate the strength of carbon transport associated with this deep Indo/Pacific loop. The ocean models typically underestimate the photosynthetic export production in the North Pacific, a problem, which is partly tied to difficulties in representing nutrient transports (Gnanadesikan et al., 2002). If the underestimate is the result of an inadequate supply of nutrients to the North Pacific from the thermocline of the South Pacific, the carbon loop would then also be significantly underestimated in the ocean general circulation models (OGCMs). Failure to simulate the relevant transport of thermocline and intermediate water would also impact the estimated transport when the OGCMs are used in the inverse calculations.

Included in Fig. 10 is a comparison between our stationary fluxes and the 'natural' CO_2 fluxes from the ocean inverse model of Gruber et al. Although there is broad general agreement in the pattern, discrepancies can be noted in several zones. In the tropical zone, for example, our fluxes have 30–100% more outgassing. In this zone our estimates are perhaps not particularly reliable, as they ultimately depend on the assumed spatial distributions of tropical outgassing, which is unconstrained by the sparse atmospheric network. Any excess tropical outgassing must be compensated in our analysis by enhanced uptake in the extratropics. Although significant differences are also evident in certain extra-tropical zones (e.g. So. Temperate and Boreal), what is most significant is their overall contribution to interhemispheric transport, discussed previously. Here we would defend our approach as adding important additional information. Estimates of air–sea fluxes based on ocean models, inversion studies and pCO_2 data all have serious limitations in the Southern Ocean ((Gruber et al., 2009), raising the possibility that these approaches cannot yet reliably resolve a critical contribution to interhemispheric carbon transport, involving natural CO_2 releases in the Southern Ocean balanced by widespread uptake throughout the rest of the worlds oceans. By relying on $\delta^{13}C$ data, our approach may help avoid this limitation.

A further process complicating the comparison of ocean- and atmospheric-based estimates is the carbon transport by rivers (Sarmiento and Sundquist, 1992). Rivers transport carbon of atmospheric origin in both inorganic and organic forms, derived from photosynthetic uptake and weathering of carbonates and silicates on land. In steady-state, the carbon delivered by rivers to the oceans minus burial must be balanced by a return flux of CO_2 from the ocean to the atmosphere. Most of the river input to the ocean is in the Northern Hemisphere. Jacobson et al. (2007) estimated that the global effective input of river carbon to the open ocean is 0.45+/–0.18 PgC yr^{-1}, with 0.29 PgC as organic carbon, 0.16 PgC as inorganic carbon. Approximately 50% of this total river carbon enters the tropical oceans between 23.5°S and 23.5°N, approximately 0.12 PgC and 0.02 PgC in the northern and southern extratropics respectively.

In the ocean inversion approach, the interhemispheric transport tied to rivers is effectively counted as part of the oceanic flux, with the uptake within the each river drainage basin being represented as an atmosphere-oceanic flux in the open ocean adjacent to the river mouth. In our ^{13}C-based atmospheric inversion, the river contribution from carbonate and silicate weathering will tend to be attributed to air–sea exchanges, while the contribution from organic carbon transport will be attributed to land fluxes. Comparing our estimated interhemispheric oceanic fluxes with those estimated by Mikaloff Fletcher et al. (2007) therefore requires adding less than 0.10 PgC yr^{-1} to our estimate of interhemispheric oceanic carbon transport. The sign is backwards from what is needed to bring the estimates into agreement, but the effect appears to be rather small in any case.

7.3. *Land contribution to gradient*

Our ability to account for the stationary components of the CO_2 and $\delta^{13}C$ gradients by ocean processes alone restricts the possible behaviour of any land CO_2 sinks. Conceptually, we separate the land sink into a component that has grown roughly in proportion to fossil fuel burning and a component which has been stationary with time. The latter component is constrained by our analysis to have either been very small, or to have produced an effect on the gradient, which was largely offset by a rectifier effect.

The impact of uncertainty in the rectifier effect on the gradient has been addressed in prior work (Denning et al., 1995; Law et al., 1996; Denning et al., 1999), with that of Stephens et al. (2007) pointing to the likelihood that the rectifier contribution is quite small. Our study makes a contribution to this discussion, by clarifying that a large rectifier, such as that simulated in the

CSU model, requires not just a large land sink in recent decades, but also requires a persistent large land sink over the past half century. Because such a large persistent sink seems doubtful on various grounds, our study indirectly strengthens the case for a small rectifier contribution.

An important question is whether our standard inversion calculation (STND_INV) satisfies the constraints on the vertical profile introduced by Stephens et al. (2007) using aircraft data in the Northern Hemisphere. To evaluate atmospheric transport models, Stephens et al. compared the predicted and observed vertical profiles of CO_2 with transport model estimates of this gradient. Among the models evaluated was a version of the TM2 model, which performed relatively well. We also tested our version of TM2 using the Stephens et al. vertical profiles and found (not shown) that TM2 tended to underestimate the gradient below ∼3000 m and overestimate the gradient above 3000 m, so that the overall difference between the near surface and the upper troposphere was well simulated. The implication is that the version of TM2 used here lies within the range of the better performing models and that the real atmosphere has a small rectifier effect, similar to TM2. However, the Stephens study suggests that the TM2 rectifier might be too small by as much as 0.4–0.5 ppm. Scaling this offset by the northern sink/rectifier ratio (computed from the difference between the STND_INV and REC2_INV calculations), suggests that the total northern land sink in the STND_INV calculation may be too small by as much as 0.2–0.3 PgC yr^{-1} owing to a possible underestimate of the seasonal rectifier.

Our analysis leaves open the possibility of a northern land sink, which has grown over time along with fossil fuel burning. The STND_INV calculation requires a substantial contemporary land sink in northern latitudes of 1.7 PgC yr^{-1} in 2003, and 1.6 PgC yr^{-1} for the 1992–1996 period. We can compare our 1992–1996 estimate to a range of 0.5–4.0 PgC yr^{-1} found across 12 transport models and model variants in TRANSCOM3 comparison studies (Gurney et al., 2004) and a preferred estimate of 1.7 PgC yr^{-1} cited in the IPCC 4th Assessment Report (Denman et al., 2007) based on the inversions of Gurney et al. (2002, 2003), Roedenbeck et al. (2003) and Peylin et al. (2005).

Our analysis points out, however, that the magnitude of this growing land sink is highly sensitive to fine details in the dispersal of fossil fuel CO_2. We find that when we scale down the atmospheric response to fossil fuel emissions to 92% at all locations (FOS3_INV calculation) the northern land sink was reduced from 1.7 PgC yr^{-1} to 1.3 PgC yr^{-1}. Furthermore, when we set the fossil fuel response equal to the regression values at each station individually (FOS2_INV calculation), the northern land sink decreases dramatically to 0.3 PgC yr^{-1}. The sensitivity to finer spatial details of the dispersal might result in part from the small number of regions that we use in our study, but suggests that efforts to more finely resolve the fossil fuel emissions source as in the Vulcan project (Graven et al., 2009; Gurney et al., 2009), and to use radiocarbon measurements as an additional tracer in atmospheric studies (Graven et al., 2009) are warranted.

If we discount the possibility of a large rectifier effect, our estimates of the northern land sink for year 2003 range from 0.3 to 1.7 PgC yr^{-1}. An almost identical range is found by bottom-up estimates, which range from 0.36 to 1.6 PgC yr^{-1} based on a compilation of regional studies from Canada, China, the United States, Europe and Russia (Denman et al., 2007). Both approaches allow that the northern land sink might be as small as 0.4 PgC yr^{-1}. The reality of a large northern sink is therefore apparently still conjectural.

8. Acknowledgments

Authors CDK and TPW passed away in June and September 2005, respectively. At that time, substantial work had been completed on this paper by CDK (data analysis, modelling, interpretation and writing), Piper (interpretation and modelling) and TPW (data analysis), and a preliminary draft had been written by CDK. Preliminary versions of this work were presented orally by CDK in various forums in 2004 and 2005, and by SCP at the 7th International Carbon Dioxide Conference in September 2005. Subsequently, RFK and SCP revisited the basic arguments, carried out additional sensitivity tests and added new Figs 3, 6–13 and Tables 1–5. Most of the text up to and

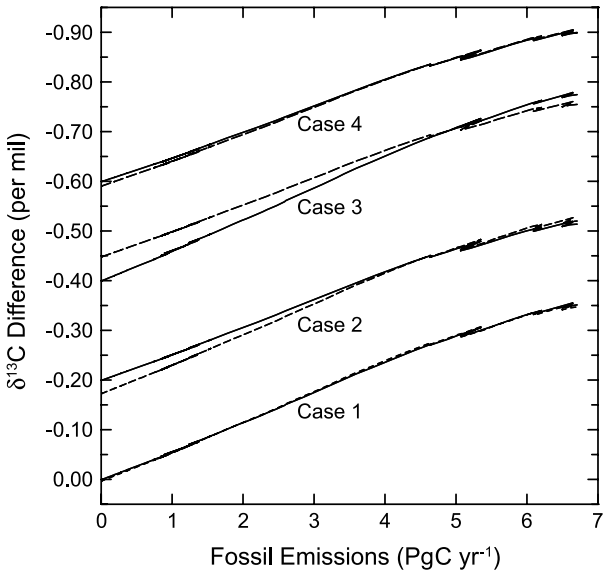

Fig. 13. The predicted change in the $\delta^{13}C$ gradient (Barrow minus South Pole) versus fossil fuel emissions based on forward model runs (solid) and regressions to these runs using eq. (2) (dashed). Four cases are shown, offset vertically by −0.020, −0.040 and −0.060 per mil. Case 1 includes the following components in the forward run: fossil fuel emissions (FOS), perturbation ocean sink (EXC), oceanic Suess effect (OSU) and biospheric Suess effect (BSU) (see Table 4). Case 2 includes FOS + EXC, Case 3 FOS + OSU and Case 4 FOS + BSU.

including Section 4 was written by CDK. All the remaining text, including the Abstract and Appendix, was written by SCP and RFK. We thank Lynne Merchant for help with figures and Lisa Welp for helpful comments. This material is based in part upon work supported by the U.S. National Science Foundation under grants ATM01–20527 and ATM06–32770, by the U.S. Department of Energy under DE-FG02–04ER63898 and DE-FG02–07ER64362 and by NASA under NAG5–11217 and NNG06GB98G. Any opinions, findings and conclusions or recommendations expressed in this material are those of the authors and do not necessarily reflect the views of NSF, DOE or NASA.

9. Appendix A: Consistency of regressions

Our approach to deriving the stationary isotopic gradient involves extrapolating the contemporary δ^{13}C gradient to zero fossil fuel burning using eq. (2). As described in Section 3.2, eq. (2) provides a reasonable fit to the observations since 1978, but this is not sufficient to demonstrate that it can be extrapolated to earlier times. Equation (2) assumes that the CO_2 and δ^{13}C gradients contain a component that increases in proportion to fossil fuel burning and that this δ^{13}C component is related to the corresponding component in CO_2 concentration as expected from the isotopic composition of fossil fuels. Equation (2) neglects the influence of the net uptake of CO_2 by the ocean, which steepens the CO_2 gradient, due to the predominance of ocean area in the Southern Hemisphere, but has little influence on δ^{13}C. It also neglects the contribution of net isotopic exchange fluxes (i.e. isofluxes) with the land and ocean, which can influence δ^{13}C but no net effect on CO_2 concentration. A key question is whether the extrapolation based on eq. (2) is justifiable in light of these additional exchanges.

To examine the influence of these other processes, we use synthetic data generated from the global reservoir model (described in Section 4.1 in the context of the single deconvolution analysis). We run the reservoir model in 'forward' mode, starting from a pre-industrial steady-state, which is then perturbed by fossil fuel CO_2 emissions. The reservoir model yields estimates of the time-varying net flux of CO_2 into the ocean as well as the isofluxes with the land and oceans. These terms (forward equivalents of EXC, BSU, OSU, FOS, see Appendix B) are then scaled by the atmospheric responses from the TM2 transport model for each of these source components and summed to yield estimates of the time-varying CO_2 concentration and δ^{13}C at the stations. By construction, the synthetic gradients in CO_2 and δ^{13}C start at zero and grow with time.

To test whether eq. (2) can account for these synthetic data, we apply the regression analysis to each station for the period 1978–2003. We then examine whether this regression extrapolates reliably to yield zero δ^{13}C difference pre-industrially. Any non-zero stationary value is a rough measure of the expected error in extrapolation using eq. (2).

The results for Barrow (minus South Pole) are shown in Fig. 13. The close agreement between the fit and the synthetic data confirms that eq. (2) can reliably be extrapolated backwards before 1978.

To help understand why the approach is so successful, we generated three additional synthetic data sets that include the FOS term but only one of the EXC, BSU or OSU terms. The synthetic time series of atmospheric δ^{13}C at Barrow for each of these cases is also shown in Fig. 13. For the FOS + EXC case, the extrapolation for Barrow is too positive (low in graph) by 0.03 per mil, for the FOS + OSU case the extrapolation is too negative by 0.05 per mil, and for the FOS + BSU case, the extrapolation is too positive by 0.01 per mil. Therefore, the success for the full case (FOS + EXC + BSU + OSU) evidently hinges on the cancellation of various contributions, particularly the contributions from the OSU and the EXC terms.

The degree of cancellation is sensitive to modelling errors in the EXC, BSU and OSU terms. These terms are unlikely to be in error by more than 30% of their magnitude, and the sign of each term is unambiguous. The total contribution of these terms to the errors in extrapolation using eq. (2), is therefore likely no larger than 0.02 per mil.

This synthetic analysis has not treated a possible contribution to the CO_2 gradients via a net land biospheric source or sink of CO_2. However, to the extent that a land biospheric component contributes to the time-varying CO_2 gradient, it will also contribute to the δ^{13}C gradient with essentially the same scaling as fossil fuel burning. Such a component would thus be indistinguishable from fossil fuel burning, using eq. (2) and would not influence the extrapolation.

Appendix B

B.1. Inverse model source components

The model source components for the inverse model calculation were taken from Piper et al. (2001). A brief description of each component follows.

B.2. Fossil fuel (industrial) emissions: FOS

Fossil fuel emissions are distributed based on 1 × 1 degree distributions for 1980 and 1990 given by Andres et al. (1996b,c, 2000). Seasonality in each grid cell north of 23.5°N is based on monthly percentages of the annual total as determined by Rotty (1987) for 1982, and with opposite phase assumed south of 23.5°S, and no seasonality in the tropics. Annual global source strengths are as specified by Boden et al. (1996) and updates. The isotopic composition of the emissions is as specified by Andres et al. (2000), applied globally, uniformly in space and time for each year.

B.3. Perturbation ocean sink: EXC

The ocean sink from the single deconvolution is distributed over the sea surface in proportion to the air–sea CO_2 exchange coefficient of Heimann and Monfray (1989). The isotopic composition is a function of kinetic and equilibrium isotopic fractionation factors that are invariant in space and time, and the isotopic composition of the ocean-mixed layer, which is globally uniform but varies in time according to the global deconvolution (Piper et al., 2001).

B.4. Adjustable zonal oceanic source components: OCE1, OCE2 and OCE3

The strengths of the three zonal oceanic components are determined by inverse calculation. The extents of these components are the ice-free ocean from 90°S–23.5°S (OCE1), 23.5°S–23.5°N (OCE2) and 23.5°N–90°N (OCE3) (Piper et al., 2001). OCE2, is distributed spatially as described in Heimann and Keeling (1989) and Piper et al. (2001), to account for important variations in ΔpCO_2 latitude and longitude. Isotopic composition of these sources is the same as for source component EXC above.

Note that we have distributed all regional and global ocean source components (EXC, OCE1, OCE2, OCE3 and ATL) in proportion to the air–sea CO_2 exchange coefficient of (Heimann and Monfray, 1989), which were calculated from wind speeds from ship reports and meteorological analyses, and climatological sea surface temperatures with the Liss and Merlivat (1986) gas exchange parameterization, and scaled up to match global mean exchange estimated from uptake of bomb-produced radiocarbon or the natural radiocarbon balance.

The contemporary air–sea CO_2 fluxes in our standard inverse calculation for year 2000 are similar in latitudinal distribution to the contemporary air–sea CO_2 fluxes reported recently by Takahashi et al. (2009) for nominal year 2000, expressed as percentages of the global total in each 4° latitudinal zone, with a mean absolute deviation of 1.3% of the global total flux, with two exceptions in the south: at 36–48°S, where there is substantially more uptake in the Takahashi data set (maximum difference of 10% of the global total at 40°S) and at 60°S, where there is more outgassing in Takahashi by about 5% of the global total.

B.5. North Atlantic sink: ATL

The North Atlantic sink component is set to -0.7 PgC yr^{-1} in the north Atlantic Ocean north of 23.5°N, with a compensating source south of 39°S (Heimann and Keeling, 1989; Piper et al., 2001). The isotopic composition of this source is the same as for source component EXC above.

B.6. Seasonal oceanic CO_2 exchange: TDE

The TDE component accounts for CO_2 exchange between air and sea produced by seasonal changes of temperature in surface sea water, with adjustments to account in part for biological activity. At low to mid-latitudes, pCO_{2sea} is set to vary seasonally with temperature according to the chemical relationship of Weiss et al. (1982), and poleward the seasonality is linearly reduced to zero. The seasonal exchange is normalized in each model grid cell to produce a zero net annual flux. The isotopic composition of this source is the same as for source component EXC above.

B.7. Oceanic ^{13}C Suess effect: OSU

The inversion calculations specify the global time-varying isotopic exchange between the atmosphere and ocean driven by the changing atmospheric $^{13}C/^{12}C$ ratio based on the single deconvolution calculation, with the exchange distributed over the sea surface in proportion to the air–sea exchange efficient of Heimann and Monfray (1989).

B.8. Equilibrium temperature-dependent fractionation: TDF

The temperature-dependent fraction of ^{13}C and ^{12}C of CO_2 exchanged between air and sea is specified by

$$^{*}F_{\mathrm{TDF}}(x,t) = k_{\mathrm{ex}}(x,t)\cdot R_s\cdot\alpha_{\mathrm{am}}\cdot(1+\delta_m)\cdot <\overline{p\mathrm{CO}_{2\mathrm{sea}}}> \cdot(\alpha_{\mathrm{eq}}(x,t) - <\overline{\alpha_{\mathrm{eq}}}>),$$

where $k_{\mathrm{ex}}(x,t)$ is the seasonally and spatially varying air–sea exchange coefficient, R_s the $^{13}C/(^{12}C + {}^{13}C)$ ratio of the PDB standard, α_{am} the kinetic fractionation factor for exchanges from air to sea, δ_m the reduced isotopic ratio of the ocean mixed layer from the global deconvolution, $<\overline{p\mathrm{CO}_{2\mathrm{sea}}}>$ the global average pCO_2 of the ocean-mixed layer, $\alpha_{\mathrm{eq}}(x,t)$ the seasonally and spatially varying equilibrium fractionation factor, and $<\overline{\alpha_{\mathrm{eq}}}>$ the globally and annually averaged equilibrium factor. The value $pCO_{2\mathrm{sea}}$ is set to the globally averaged pCO_2 in the atmosphere as specified by global deconvolution (Heimann and Keeling, 1989).

B.9. Seasonal biospheric exchange: SBE

Purely SBE in the model includes contributions from net primary production (NPP) and heterotrophic respiration (RES). NPP is specified by a light efficiency model using Pathfinder NDVI data for 1982–1990 (James and Kalluri, 1994) and PAR processed for the year 1986 (Pinker and Laszlo, 1992). Heterotrophic respiration is specified as a function of daily surface air temperature for the year 1986 (Piper and Stewart, 1996). The light efficiency factor and seasonal fraction of RES were adjusted to provide a best fit to CO_2 observations for 1986 at Point Barrow, Alaska,

La Jolla, California and Cape Kumukahi, Hawaii, and to give a zero annual net flux for the sum of the seasonal components NPP and RES in each grid cell. The isotopic composition of the photosynthetic flux (NPP component) is isotopically depleted relative to the atmospheric CO_2 reservoir based on a fixed fractionation factor of −15.32 per mil; it is assumed to be uniform in space but to vary year to year as a function of the isotopic composition of the atmospheric reservoir. The isotopic composition of respiration is prescribed to be identical to photosynthesis.

B.10. Land biospheric ^{13}C Suess effect: BSU

The inversion calculations specify the global time-varying isotopic exchange between the atmosphere and land biosphere driven by the changing atmospheric $^{13}C/^{12}C$ ratio based on the single deconvolution calculation, with the exchange distributed over the land surface in proportion to NPP, as specified for the SBE component above. The net effect of the terrestrial Suess effect is to shift the isotopic composition of respiration relative to isotopic composition of contemporaneous NPP.

B.11. Biospheric fertilization: FER

The component FER was distributed using the spatial distribution of NPP determined above. Its global strength was specified by the global deconvolution. Its isotopic composition is assumed to the same as global respiration, allowing for the ^{13}C Suess effect (see above).

B.12. Biospheric destruction: DES

The component for deforestation and land use changes, DES, was distributed in 12 regions according to Houghton et al. (1987); the distribution within the regions was specified by the NPP distribution described above. The global strength was specified to be constant at 2 PgC yr^{-1}. Any error in this source tends to be compensated for by adjustments of the zonal biospheric sources. Its isotopic composition is assumed to be the same as that of the NPP, but offset by the global average terrestrial Suess effect.

B.13. Adjustable zonal biospheric source components: BIO1,2,3,4

Four zonal components distributed in the far northern latitudes (47–90°N), northern mid-latitudes (23.5–47°N), tropical (23.5°S–23.5°N) and southern mid-latitudes (23.5–47°S) (Piper et al., 2001). Each component is distributed in proportion to annual NPP (averaged from 1982–1990), and has the same seasonality as the NPP source component. The total strength of each zonal source was adjusted by the inverse calculation to achieve a best fit to atmospheric observations. The isotopic composition of each of these sources is set equal to the average of compositions for NPP and respiration fluxes; the photosynthetic discrimination in each zone varies according to the proportion of NPP owing to C3 and C4 plants (Keeling et al., 2001); specifically, photosynthetic discrimination was set to 17.80, 16.55, 14.00 and 15.35 per mil for 47–90°N, 23.5–47°N, 23.5°S–23.5°N and 23.5–47°S, respectively. The isotopic composition is assumed to be spatially uniform within each zone, but varies annually as prescribed by the global deconvolution.

References

Andres, R. J., Marland, G. and Bischof, S. 1996a. *Global and Latitudinal Estimates of δ^{13} C from Fossil-fuel Consumption and Cement Manufacture*. Carbon Dioxide Information and Analysis Center, Oak Ridge, Tennessee.

Andres, R. J., Marland, G., Fung, I. Y. and Matthews, E. 1996b. A one degree by one degree distribution of carbon dioxide emissions from fossil-fuel consumption and cement manufacture, 1950–1990. *Global Biogeochem. Cycles* **10**, 419–429.

Andres, R. J., Marland, G., Fung, I. Y. and Matthews, E. 1996c. *One Degree by One Degree Patterns of Carbon Dioxide Emissions From Fossil-Fuel Burning, Hydraulic Cement Production, and Gas Flaring on a One Degree by One Degree Grid Cell Basis: 1950 to 1990*. Carbon Dioxide Analysis Center, Oak Ridge, Tennessee.

Andres, R. J., Marland, G., Boden, T. A. and Bischof, S. 2000. Carbon dioxide emissions from fossil fuel consumption and cement manufacture, 1751–1991, and an estimate of their isotopic composition and latitudinal distribution. In: *The Carbon Cycle* (eds T. M. L. Wigley and D. S. Schimel). Cambridge University Press, Cambridge, 53–62.

Bacastow, R. B., Keeling, C. D. and Whorf, T. P. 1985. Seasonal Amplitude Increase in Atmospheric CO_2 Concentration at Mauna Loa, Hawaii, 1959–1982. *J. Geophys. Res.-Atmos.* **90**, 10 529–10 540.

Bevington, P. R. 1969. *Data Reduction and Error Analysis for the Physical Sciences*. McGraw-Hill Book Co, New York, NY.

Boden, T. A., Marland, G. and Andres, R. J. 1996. *Estimates of Global, Regional, and National Annual CO_2 Emissions from Fossil-Fuel Burning, Hydraulic Cement Production, and gas flaring: 1950–1992*. Oak Ridge National Laboratory, Oak Ridge, Tennessee, 1–600.

Bolin, B. and Keeling, C. D. 1963. Large-scale atmospheric mixing as deduced from seasonal and meridional variations of carbon dioxide. *J. geophys. Res.* **68**, 3899–3920.

Conway, T. and Tans, P. P. 1999. Development of the CO_2 latitude gradient in recent decades. *Global Biogeochem. Cycles* **13**, 821–826.

Denman, K. L., Brasseur, G., Chidthaisong, A., Ciais, P., Cox, P. M. and co-authors. 2007. Couplings between changes in the climate system and biogeochemistry. In: *Climate Change 2007: The Physical Science Basis. Contribution of Working Group I to the Fourth Assessment Report of the Intergovernmental Panel on Climate Change* (eds S. Solomon, D. Qin, M. Manning, Z. Chen, M. Marquis and co-authors). Cambridge University Press, Cambridge, United Kingdom and New York, NY, USA.

Denning, A. S., Fung, I. Y. and Randall, D. 1995. Latitudinal gradient of atmospheric co$_2$ due to seasonal exchange with land biota. *Nature* **376**, 240–243.

Denning, A. S., Takahashi, T. and Friedlingstein, P. 1999. Can a strong atmospheric CO_2 rectifier effect be reconciled with a "reasonable" carbon budget? *Tellus* **51B**, 249–253.

Doney, S. C., Lindsay, K., Caldeira, K., Campin, J. M., Drange, H. and co-authors. 2004. Evaluating global ocean carbon models: the importance of realistic physics. *Global Biogeochem. Cycles* **18**, doi:10.1029/2003GB002150.

Doney, S. C., Lindsay, K., Fung, I. and John, J. 2006. Natural variability in a stable, 1000-yr global coupled climate-carbon cycle simulation. *J. Clim.* **19**, 3033–3054.

Fan, S. M., Blaine, T. L. and Sarmiento, J. L. 1999. Terrestrial carbon sink in the Northern Hemisphere estimated from the atmospheric CO_2 difference between Mauna Loa and the South Pole since 1959. *Tellus* **51B**, 863–870.

Gloor, M., Gruber, N., Sarmiento, J., Sabine, C. L., Feely, R. A. and co-authors. 2003. A first estimate of present and preindustrial air-sea CO_2 flux patterns based on ocean interior carbon measurements and models. *Geophys. Res. Lett.* **30**, art. no.-1010.

Gnanadesikan, A., Slater, R. D., Gruber, N. and Sarmiento, J. L. 2002. Oceanic vertical exchange and new production: a comparison between models and observations. *Deep-Sea Res. Part II-Top. Stud. Oceanogr.* **49**, 363–401.

Graven, H. D., Stephens, B. B., Guilderson, T. P., Campos, T. L., Schimel, D. S. and co-authors. 2009. Vertical profiles of biospheric and fossil fuel-derived CO_2 and fossil fuel CO_2 : CO ratios from airborne measurements of Delta C-14, CO_2 and CO above Colorado, USA. *Tellus* **61B**, 536–546.

Gruber, N., Gloor, M., Fletcher, S. E. M., Doney, S. C., Dutkiewicz, S. and co-authors. 2009. Oceanic sources, sinks, and transport of atmospheric CO_2. *Global Biogeochem. Cycles* **23**, doi: 10.1029/2008GB003349.

Gurney, K. R., Law, R. M., Denning, A. S., Rayner, P. J., Baker, D. and co-authors. 2002. Towards robust regional estimates of CO_2 sources and sinks using atmospheric transport models. *Nature* **415**, 626–630.

Gurney, K. R., Law, R. M., Denning, A. S., Rayner, P. J., Baker, D. and co-authors. 2003. TransCom 3 CO_2 inversion intercomparison: 1. Annual mean control results and sensitivity to transport and prior flux information. *Tellus* **55B**, 555–579.

Gurney, K. R., Law, R. M., Denning, A. S., Rayner, P. J., Pak, B. C. and co-authors. 2004. Transcom 3 inversion intercomparison: model mean results for the estimation of seasonal carbon sources and sinks. *Global Biogeochem. Cycles* **18**, doi:10.1029/2003GB002111.

Gurney, K. R., Mendoza, D. L., Zhou, Y. Y., Fischer, M. L., Miller, C. C. and co-authors. 2009. High resolution fossil fuel combustion CO_2 emission fluxes for the United States. *Environ. Sci. Technol.* **43**, 5535–5541.

Heimann, M. and Keeling, C. D. 1989. A three-dimensional model of atmospheric CO_2 transport based on observed winds: 2. Model description and simulated tracer experiments. In: *Aspects of Climate Variability in the Pacific and the Western Americas* (ed. D. H. Peterson). American Geophysical Union, Washington, D.C., 237–275.

Heimann, M. and Monfray, P. 1989. *Spatial and Temporal Variation of The Gas Exchange Coefficient for CO_2: 1. Data Analysis and Global Validation*. Max Planck Institute for Meteorology, Hamburg, 1–29.

Heimann, M. 1995. The global atmospheric tracer model TM2. In: *Deutsches Klimarechenzentrum Technical Report*. Hamburg, Germany, 1–53.

Houghton, R. A., Boone, R. D., Fruci, J. R., Hobbie, J. E., Melillo, J. M. and co-authors. 1987. The flux of carbon from terrestrial ecosystems to the atmosphere in 1980 due to changes in land use: geographic distribution of the global flux. *Tellus* **39B**, 122–139.

Jacobson, A. R., Fletcher, S. E. M., Gruber, N., Sarmiento, J. L. and Gloor, M. 2007. A joint atmosphere-ocean inversion for surface fluxes of carbon dioxide: 2. Regional results. *Global Biogeochem. Cycles* **21**, doi:10.1029/2006GB002703.

James, M. E. and Kalluri, S. N. V. 1994. The Pathfinder AVHRR land data set–an improved coarse resolution data set for terrestrial monitoring. *Int. J. Remote Sens.* **15**, 3347–3363.

Keeling, C. D. and Heimann, M. 1986. Meridional Eddy Diffusion Model of the transport of atmospheric carbon dioxide 2. Mean annual carbon cycle. *J. geophys. Res.-Atmos.* **91**, 7782–7796.

Keeling, C. D., Bacastow, R. B., Carter, A. F., Piper, S. C., Whorf, T. P. and co-authors. 1989a. A three-dimensional model of atmospheric CO_2 transport based on observed winds: 1. Analysis of observational data. In: *Aspects of Climate Variability in the Pacific and the Western Americas*. (ed. D. H. Peterson). American Geophysical Union, Washington, D.C., 165–236.

Keeling, C. D., Guenther, P. R. and Whorf, T. P. 1989b. *An Analysis of the Concentration of Atmospheric Carbon Dioxide at Fixed Land Stations, and Over the Oceans Based on Discrete Samples and Daily Averaged Continuous Measurements*. Scripps Institution of Oceanography, La Jolla, CA, U.S.A., 1–451.

Keeling, C. D., Piper, S. C. and Heimann, M. 1989c. A three-dimensional model of atmospheric CO_2 transport based on observed winds: 4. Mean annual gradients and interannual variations. In: *Aspects of Climate Variability in the Pacific and the Western Americas* (ed. D. H. Peterson). American Geophysical Union, Washington, D.C., 305–363.

Keeling, C. D., Piper, S. C., Bacastow, R. B., Wahlen, M., Whorf, T. P. and co-authors. 2001. Exchanges of atmospheric CO_2 and $^{13}CO_2$ with the terrestrial biosphere and oceans from 1978 to 2000. In: *Scripps Institution of Oceanography References Series*. Scripps Institution of Oceanography, La Jolla, CA, 1–89.

Keeling, C. D., Piper, S. C., Bacastow, R. B., Wahlen, M., Whorf, T. P. and co-authors. 2005. Atmospheric CO_2 and $^{13}CO_2$ exchange with the terrestrial biosphere and oceans from 1978 to 2000: observations and carbon cycle implications. In: *A History of Atmospheric CO_2 and Its Effects on Plants, Animals, and Ecosystems*. (eds J. R. Ehleringer, T. E. Cerling and M. D. Dearing). Springer, New York, 83–113.

Kelley, J. J. Jr, 1969. An analysis of carbon dioxide in the arctic atmosphere near Barrow, Alaska 1961 to 1967. Contract N00014-67-A-0103-0007 NR 307–252, Scientific report of the United States Office of Naval Research, 172.

Law, R. M., Rayner, P. J., Denning, A. S., Erickson, D., Fung, I. Y. and co-authors. 1996. Variations in modeled atmospheric transport of carbon dioxide and the consequences for CO_2 inversions. *Global Biogeochem. Cycles* **10**, 783–796.

Liss, P. S. and Merlivat,L. 1986. Air-sea exchange rates: introduction and synthesis. In: *The Role of Air-Sea Exchange in Geochemical Cycling* (ed. P. Buat-Menard). Reidel, Dordrecht, 113–127.

Marland, G., Boden, T. A. and Andres, R. J. 2005. Global, regional, and national fossil fuel CO_2 emissions. In: *Trends: A Compendium of Data on Global Change*. Carbon Dioxide Analysis Center, Oak Ridge National Laboratory, U.S. Department of Energy, Oak Ridge, Tennessee, U.S.A.

Mikaloff Fletcher, S. E., Gruber, N., Jacobson, A. R., Gloor, M., Doney, S. C. and co-authors. 2007. Inverse estimates of the oceanic sources

and sinks of natural CO_2 and the implied oceanic carbon transport. *Global Biogeochem. Cycles* **21**, doi: 10.1029/2006GB002751.

Mikaloff Fletcher, S. E., Gruber, N. P. and Jacobson, A. R. 2003. *Ocean Inversion Project How-to Document Version 1.0*. Institution for Geophysics and Planetary Physics, The University of California, Los Angeles, CA, 18 pp.

Mook, W. G., Koopmans, M., Carter, A. F. and Keeling, C. D. 1983. Seasonal, latitudinal, and secular variations in the abundance and isotopic ratios of atmospheric carbon dioxide 1. Results from land stations. *J. geophys. Res.-Oceans and Atmospheres* **88**, 915–933.

Peylin, P., Bousquet, P., Le Quere, C., Sitch, S., Friedlingstein, P. and co-authors. 2005. Multiple constraints on regional CO_2 flux variations over land and oceans. *Global Biogeochem. Cycles* **19**, doi:10.1029/2003GB002214.

Pinker, R. T. and Laszlo, I. 1992. Modeling surface solar irradiance for satellite applications on a global scale. *J. appl. Meteorol.* **31**, 194–211.

Piper, S. C. and Stewart, E. F. 1996. A gridded global data set for daily temperature and precipitation for terrestrial biospheric modelling. *Global Biogeochem. Cycles* **10**, 757–782.

Piper, S. C., Keeling, C. D., Heimann, M. and Stewart, E. F. 2001. Exchanges of Atmospheric CO_2 and $^{13}CO_2$ with the Terrestrial Biosphere and Oceans from 1978 to 2000 II. In: *A Three-Dimensional Tracer Inversion Model to Deduce Regional Fluxes*. Scripps Institution of Oceanography, La Jolla, CA, USA, 1–57.

Robbins, P. E. and Bryden, H. L. 1994. Direct observations of advective nutrient and oxygen fluxes at 24 Degrees N in the Pacific Ocean. *Deep-Sea Research Part I-Oceanographic Research Papers* **41**, 143–168.

Roedenbeck, C., Houweling, S., Gloor, M. and Heimann, M. 2003. CO_2 flux history 1982–2001 inferred from atmospheric data using a global inversion of atmospheric transport. *Atmos. Chem. Phys.* **3**, 1919–1964.

Rotty, R. M. 1987. Estimates of seasonal variation in fossil fuel CO_2 emissions. *Tellus* **39B**, 184–202.

Sarmiento, J. L. and Sundquist, E. T. 1992. Revised budget for the oceanic uptake of anthropogenic carbon dioxide. *Nature* **356**, 589–593.

Stephens, B. B., Gurney, K. R., Tans, P. P., Sweeney, C., Peters, W. and co-authors. 2007. Weak northern and strong tropical land carbon uptake from vertical profiles of atmospheric CO_2. *Science* **316**, 1732–1735.

Takahashi, T., Sutherland, S. C., Sweeney, C., Poisson, A., Metzl, N. and co-authors. 2002. Global sea-air CO_2 flux based on climatological surface ocean pCO_2, and seasonal biological and temperature effects. *Deep-Sea Research Part II-Topical Studies in Oceanography* **49**, 1601–1622.

Takahashi, T., Sutherland, S. C., Wanninkhof, R., Sweeney, C., Feely, R. A. and co-authors. 2009. Climatological mean and decadal change in surface ocean pCO_2, and net sea-air CO_2 flux over the global oceans. *Deep-Sea Research Part II-Topical Studies in Oceanography* **56**, 554–577.

Taylor, J. A. and Orr, J. C. 2000. The natural latitudinal distribution of atmospheric CO_2. *Glob. Planet. Change* **26**, 375–386.

Weart, S. R. 2003. *The Discovery of Global Warming*. Harvard University Press, Cambridge, MA.

Weiss, R. F., Jahnke, R. A. and Keeling, C. D. 1982. Seasonal effects of temperature and salinity on the partial pressure of CO_2 in sea-water. *Nature* **300**, 511–513.